NASA TECHNICAL NOTE

CRITICAL-SPEED ANALYSIS OF FLEXIBLY MOUNTED RIGID ROTORS

by Richard H. Cavicchi

Lewis Research Center

Cleveland, Ohio

NATIONAL AERONAUTICS AND SPACE ADMINISTRATION • WASHINGTON, D. C. • JUNE 1968

CRITICAL-SPEED ANALYSIS OF FLEXIBLY MOUNTED RIGID ROTORS

By Richard H. Cavicchi

Lewis Research Center
Cleveland, Ohio

NATIONAL AERONAUTICS AND SPACE ADMINISTRATION

ABSTRACT

A general solution of the frequency equation for rigid rotors in undamped bearings is derived for forward and backward precession. The solution is applied to a wide range of speeds and shapes, with variation in center-of-gravity location, to obtain maps of the frequency characteristics and locate major and nonsynchronous critical speeds. When the center of gravity is at the bearing centerline midpoint, a set of two solutions exists. An additional set of two solutions appears, however, when the center of gravity is away from this point. No forward-precession high-frequency critical speeds exist if the moment-of-inertia ratio equals or exceeds the critical-speed ratio. With the center of gravity midway between single-row ball bearings and the polar and diametral moments of inertia equal, a nonsynchronous critical speed exists at all rotor speeds.

STAR Category 32

CONTENTS

CRITICAL-SPEED ANALYSIS OF FLEXIBLY MOUNTED RIGID ROTORS

by Richard H. Cavicchi

Lewis Research Center

SUMMARY

A theoretical analysis of rigid rotors in undamped flexible bearings develops and solves a general frequency equation to determine frequencies of both forward and backward precession. This study applies the general solution to a wide range of rotor rotational speeds and to shapes that vary from a pencil shape to a disk. The center of gravity varies from midway between the bearings to an outboard quarter point. Maps present the frequency characteristics of all these configurations for use as a guide in preliminary design. Besides locating major critical speeds, the maps locate numerous nonsynchronous critical speeds that may result from bearing defects.

A single two-branch curve completely describes a set of two solutions for all shapes when the center of gravity lies midway between the bearings. With this location between single-row ball bearings and the polar and diametral moments of inertia equal, a nonsynchronous critical speed exists at all rotor speeds. When the center of gravity is away from the bearing centerline midpoint, two sets of solutions for forward and backward precession result. One is a low-frequency set, and the other is high. The frequency magnitude of forward precession exceeds that of backward precession in each set over all rotational speeds studied. As rotor speed increases, the frequency magnitude of forward precession increases and that of backward precession decreases.

As the center of gravity is moved progressively from the bearing centerline midpoint, major critical speeds of the low-frequency set decrease in magnitude and those of the high-frequency set increase. The effect of the center-of-gravity location on major critical speed decreases as geometries become more disk-like.

This analysis revealed that, in backward precession, disks have lower major critical speeds than pencil shapes. No forward-precession high-frequency critical speeds exist if the ratio of polar to diametral moments of inertia equals or exceeds the critical-speed ratio.

INTRODUCTION

Numerous investigators have studied the problem of vibrations in rotating machinery. Gunter (ref. 1) traces the history of some of this work over the past century. He adds his own contribution with a general study of nonsynchronous precession in a rotor system. In references 2 and 3, Yamamoto makes major advances in this field by combining theoretical and experimental treatments. He studies shafts and disks and varies the axial location and thickness of the disk. Yamamoto's work reveals that ball-bearing defects can cause critical speeds both below and above the major critical speed, the speed at which rotational and precession frequencies are equal. Dimentberg (ref. 4) also presents a variety of theoretical studies on shaft-disk systems backed by experiment. Eshleman and Eubanks report on a continuous shaft-disk system in reference 5.

Despite the thorough treatment in these references, NASA requirements have stimulated further work on rotor systems. The work of reference 6 is aimed at predicting the deflection amplitude and frequency of vibrations in an axial turbopump, the design of which is described in this reference.

The intention of the present report is to extend the prediction of vibration frequencies beyond the study of one particular machine as done in reference 6. By contrast, the work performed herein covers a wide range of rotor shapes and speeds. This report presents the results of a parametric analysis of rotor dynamic frequencies. Its purpose is to aid in preliminary design of turbomachinery by providing guidance as to the location of potential major and nonsynchronous critical speeds.

In this study, the rotor geometry varies from a pencil shape to a disk, and the rotor speed is varied over a wide range. The analysis is performed for four axial locations for the center of gravity: midway between the bearings, at inboard and outboard quarter points, and at a bearing.

The results of calculations made for this analysis are presented in the form of dimensionless working charts relating vibration frequency with speed. Shape factors are used as parameters to display the effect of geometry on critical speed. This analysis is a continuation of work suggested by Timoshenko in reference 7.

The operating conditions of the axial turbopump investigated in reference 6 are located on some of the working charts to display their proximities to various critical speeds.

DESCRIPTION OF ROTOR-BEARING SYSTEM

Figure 1 is a representation of a rigid rotor on a shaft mounted in flexible bearings. The mass of the shaft is neglected. This study considers motion in the lateral (y and z) directions, but no axial motion (x). (All symbols are defined in appendix A.) In figure 1,
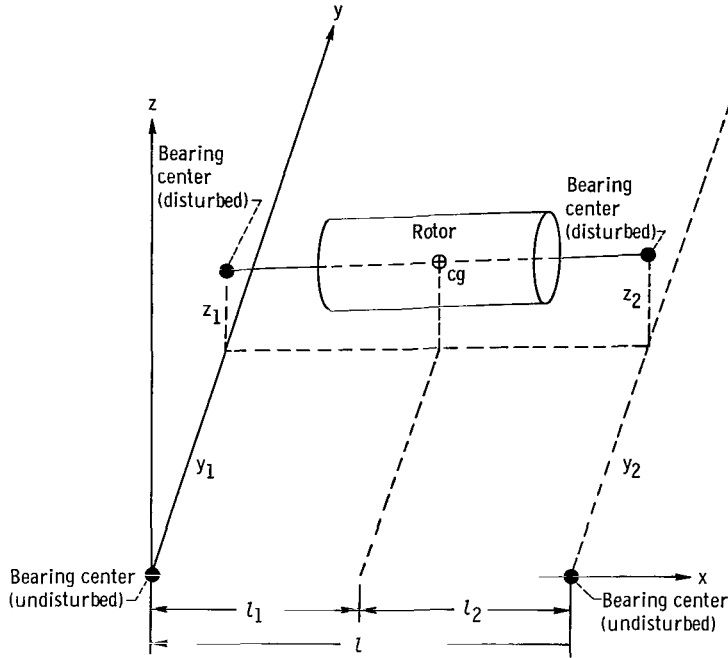
Figure 1. – Rotor-bearing system geometry.

y- and z-displacements of the shaft are greatly magnified for clarity. This study further assumes no friction, no unbalance, and no external disturbing force. Specifically, there is no damping in the bearings.

The rotor configuration varies from a pencil shape to a disk. Shape is introduced into the mathematical analysis in terms of the rotor polar moment of inertia I and its diametral moment of inertia I_1. To make the analysis nondimensional, the moments of inertia are expressed as dimensionless parameters:

$$\pi_2 = \frac{I_1}{M l^2} \tag{1}$$

$$\pi_3 = \frac{I}{I_1} \tag{2}$$

The values of these parameters are small for pencil shapes, and are larger for disks. For example, the ratio I/I_1 for a rod whose length is 10 times its diameter is 0.0149. For a disk of negligible thickness, it is 2. The parameter π_2 is the disk effect used in references 5 and 8. It is zero for a concentrated mass and is infinite for a disk having

3

all its mass distributed over a large radius. Therefore, geometries become more disk-like as π_2 and π_3 increase.

In the system studied in this report, the rotor center of gravity remains on the shaft centerline. The study does, however, investigate the effect of varying the axial location of the center of gravity. The disk effect π_2 and the moment-of-inertia ratio π_3 each vary from zero to infinity in the maps prepared from this analysis.

GENERAL ANALYSIS

Figure 1 shows the geometry used in this study. The bearings are assumed to be linear springs, with a spring constant of $k/2$ for each bearing in both lateral directions.

Equations of Motion

Timoshenko presents the equations of motion for this analysis in reference 7 (pp. 287-288):

$$\frac{M}{l}(l_2\ddot{y}_1 + l_1\ddot{y}_2) + \frac{ky_1}{2} + \frac{ky_2}{2} = 0 \tag{3}$$

$$\frac{M}{l}(l_2\ddot{z}_1 + l_1\ddot{z}_2) + \frac{kz_1}{2} + \frac{kz_2}{2} = 0 \tag{4}$$

$$I\omega\left(\frac{\dot{y}_2 - \dot{y}_1}{l}\right) - I_1\left(\frac{\ddot{z}_2 - \ddot{z}_1}{l}\right) - \frac{kl_2z_2}{2} + \frac{kl_1z_1}{2} = 0 \tag{5}$$

$$I\omega\left(\frac{\dot{z}_2 - \dot{z}_1}{l}\right) + I_1\left(\frac{\ddot{y}_2 - \ddot{y}_1}{l}\right) + \frac{kl_2y_2}{2} - \frac{kl_1y_1}{2} = 0 \tag{6}$$

This study does not consider axial motion. Equations (3) and (4) are force equations; equations (5) and (6) are summations of torque. Equations (3) to (6) completely describe the free vibrations of a rigid rotor in flexible bearings. Timoshenko suggests the solutions

$$y_1 = A \sin pt \tag{7}$$

$$y_2 = B \sin pt \tag{8}$$

$$z_1 = C \cos pt \tag{9}$$

$$z_2 = D \cos pt \tag{10}$$

In equations (7) to (10), p is the frequency of rotor vibration. Calculation of p is the objective of this analysis. This study is not concerned with determining the deflections y and z, or the amplitudes A, B, C, and D.

Substitution of equations (7) to (10) into equations (3) to (6) yields

$$A\left(\frac{k}{2} - \frac{l_2}{l} Mp^2\right) + B\left(\frac{k}{2} - \frac{l_1}{l} Mp^2\right) = 0 \tag{11}$$

$$C\left(\frac{k}{2} - \frac{l_2}{l} Mp^2\right) + D\left(\frac{k}{2} - \frac{l_1}{l} Mp^2\right) = 0 \tag{12}$$

$$-A(I\omega p) + B(I\omega p) + C\left(\frac{kl_1 l}{2} - I_1 p^2\right) - D\left(\frac{kl_2 l}{2} - I_1 p^2\right) = 0 \tag{13}$$

$$-A\left(\frac{kl_1 l}{2} - I_1 p^2\right) + B\left(\frac{kl_2 l}{2} - I_1 p^2\right) + C(I\omega p) - D(I\omega p) = 0 \tag{14}$$

In matrix form, this set becomes

$$
\begin{bmatrix}
\left(\frac{k}{2} - \frac{l_2}{l} Mp^2\right) & \left(\frac{k}{2} - \frac{l_1}{l} Mp^2\right) & 0 & 0 \\
0 & 0 & \left(\frac{k}{2} - \frac{l_2}{l} Mp^2\right) & \left(\frac{k}{2} - \frac{l_1}{l} Mp^2\right) \\
-(I\omega p) & (I\omega p) & \left(\frac{kl_1 l}{2} - I_1 p^2\right) & -\left(\frac{kl_2 l}{2} - I_1 p^2\right) \\
-\left(\frac{kl_1 l}{2} - I_1 p^2\right) & \left(\frac{kl_2 l}{2} - I_1 p^2\right) & (I\omega p) & -(I\omega p)
\end{bmatrix}
\cdot
\begin{Bmatrix}
A \\ B \\ C \\ D
\end{Bmatrix}
= 0 \tag{15}
$$

5

Frequency Equation

Nontrivial solutions of A, B, C, and D in equations (11) to (14) require that the determinant of the coefficient matrix vanish. Expansion of the determinant and collection of similar terms yield

$$(MI_1)^2 p^8 - \left[M^2 I^2 \omega^2 + 2kMI_1^2 + kM^2 I_1 \left(l_1^2 + l_2^2 \right) \right] p^6$$

$$+ \left[2kMI^2 \omega^2 + \frac{k^2 M^2}{4} \left(l_1^2 + l_2^2 \right)^2 + \frac{3k^2 MI_1}{2} \left(l_1^2 + l_2^2 \right) + k^2 MI_1 l_1 l_2 + k^2 I_1^2 \right] p^4$$

$$- \left[k^2 I^2 \omega^2 + \frac{k^3 M l^2}{4} \left(l_1^2 + l_2^2 \right) + \frac{k^3 l^2 I_1}{2} \right] p^2 + \frac{k^4 l^4}{16} = 0 \tag{16}$$

Equation (16) is the general frequency equation for the model studied in this report.

Nondimensional Frequency Equation

The following dimensionless parameters make equation (16) nondimensional and shorten its appearance:

$$\pi_1 = \frac{p}{\sqrt{\dfrac{k}{M}}} \tag{17}$$

$$\pi_2 = \frac{I_1}{M l^2} \tag{1}$$

$$\pi_3 = \frac{I}{I_1} \tag{2}$$

$$\pi_4 = \frac{\omega}{\sqrt{\dfrac{k}{M}}} \tag{18}$$

$$S = \pi_1^2 \tag{19}$$

Substitution of these parameters into equation (16) yields

$$
\pi_2^2 S^4 - \left[\pi_2^2 \pi_3^2 \pi_4^2 + 2\pi_2^2 + \pi_2 \left(\frac{l_1^2 + l_2^2}{l^2} \right) \right] S^3 + \left[2\pi_2^2 \pi_3^2 \pi_4^2 + \frac{1}{4} \left(\frac{l_1^2 + l_2^2}{l^2} \right)^2 + \frac{3\pi_2}{2} \left(\frac{l_1^2 + l_2^2}{l^2} \right) \right.
$$

$$
\left. + \pi_2 \left(\frac{l_1 l_2}{l^2} \right) + \pi_2^2 \right] S^2 - \left[\pi_2^2 \pi_3^2 \pi_4^2 + \frac{1}{4} \left(\frac{l_1^2 + l_2^2}{l^2} \right) + \frac{\pi_2}{2} \right] S + \frac{1}{16} = 0 \tag{20}
$$

Solution of Frequency Equation

Solution of the quartic equation (20) for S is inconvenient. It is simpler to solve for the shape-speed parameter $\pi_3 \pi_4$. The procedure is first to form a quadratic in π_2. Equation (20) takes the form

$$
\pi_2^2 \left[S^4 - 2S^3 + S^2 - \pi_3^2 \pi_4^2 S(S-1)^2 \right] - \pi_2 \left[\left(\frac{l_1^2 + l_2^2}{l^2} \right) S^3 - \frac{3}{2} \left(\frac{l_1^2 + l_2^2}{l^2} \right) S^2 - \left(\frac{l_1 l_2}{l^2} \right) S^2 + \frac{S}{2} \right]
$$

$$
+ \frac{1}{4} \left(\frac{l_1^2 + l_2^2}{l^2} \right)^2 S^2 - \frac{1}{4} \left(\frac{l_1^2 + l_2^2}{l^2} \right) S + \frac{1}{16} = 0 \tag{21}
$$

Factoring the coefficients of this expression yields

$$
\pi_2^2 \left[S(S-1)^2 \left(S - \pi_3^2 \pi_4^2 \right) \right] - \pi_2 S(S-1) \left[S \left(\frac{l_1^2 + l_2^2}{l^2} \right) - \frac{1}{2} \right] + \frac{1}{4} \left[\left(\frac{l_1^2 + l_2^2}{l^2} \right) S - \frac{1}{2} \right]^2 = 0 \tag{22}
$$

It is convenient to solve this quadratic in π_2 for $1/\pi_2$. The solution is

$$\frac{1}{\pi_2} = \left[\frac{4(S - 1)}{2\left(\dfrac{\ell_1^2 + \ell_2^2}{\ell^2}\right)S - 1} \right] \left(S - \delta\pi_3\pi_4\sqrt{S} \right) \tag{23}$$

The result of solving equation (23) for $\pi_3\pi_4$ yields the general solution of the frequency equation

$$\delta\pi_3\pi_4 = \sqrt{S} - \frac{2\left(\dfrac{\ell_1^2 + \ell_2^2}{\ell^2}\right)S - 1}{4\sqrt{S}\,(S - 1)\pi_2} \tag{24}$$

In equations (23) and (24), for forward precession,

$$\delta = 1 \tag{25}$$

and for backward precession,

$$\delta = -1 \tag{26}$$

The presence of the factor $(S - 1)$ in the denominator reveals that no solution exists for

$$S = 1$$

or

$$\sqrt{S} = \frac{p}{\sqrt{\dfrac{k}{M}}} = 1$$

Major Critical Speed

A major critical speed is said to occur when the magnitudes of the precession and

8

rotational frequencies are equal. Also called synchronous speed, this condition is represented mathematically by

$$\left. \begin{array}{c} r_{cr} = \dfrac{\pi_1}{\pi_4} = \pm 1 \\ \\ \\ \dfrac{p}{\omega} = \pm 1 \end{array} \right\}$$

or (27)

When this relation is used in the general solution of the frequency equation (eq. (24)), the major critical speed results as follows:

$$\frac{\omega_{cr}}{\sqrt{\dfrac{k}{M}}} = \left\{ \frac{1}{2}\left[1 + \frac{\dfrac{l_1^2 + l_2^2}{l^2}}{2\pi_2(1 - \delta\pi_3)}\right] \pm \frac{1}{2}\sqrt{\left[1 + \frac{\dfrac{l_1^2 + l_2^2}{l^2}}{2\pi_2(1 - \delta\pi_3)}\right]^2 - \frac{1}{\pi_2(1 - \delta\pi_3)}} \right\}^{1/2}$$

(28)

For backward precession ($\delta = -1$), a positive sign before the radical in equation (28) always yields the high-frequency solutions; a minus sign yields the low-frequency set. For forward precession ($\delta = 1$), the same pattern is true when $\pi_3 < 1$. When $\pi_3 > 1$, however, the effects of the signs are reversed.

Calculation Procedure

The calculation procedure uses S as an independent variable for which a range of values is assigned. This is an indirect method that evaluates the dimensionless frequency parameter π_1 from graphs. From equations (17) and (19),

$$\pi_1 = \frac{p}{\sqrt{\dfrac{k}{M}}} = \sqrt{S}$$

Appendix B applies equation (24) to the four center-of-gravity axial locations. The equations for these four cases are collected here for comparison.

Center of gravity midway between bearings, case 1 ($l_1/l = 1/2$):

$$\delta\pi_3\pi_4 = \sqrt{S} - \frac{1}{4\sqrt{S}\,\pi_2} \tag{B2}$$

Center of gravity at quarter point, case 2 ($l_1/l = 3/4$):

$$\delta\pi_3\pi_4 = \sqrt{S} - \frac{\dfrac{5S}{4} - 1}{4\sqrt{S}\,(S-1)\pi_2} \tag{B15}$$

Center of gravity at one bearing, case 3 ($l_1/l = 1$):

$$\delta\pi_3\pi_4 = \sqrt{S} - \frac{2S - 1}{4\sqrt{S}\,(S-1)\pi_2} \tag{B17}$$

Center of gravity at outboard quarter point, case 4 ($l_1/l = 5/4$):

$$\delta\pi_3\pi_4 = \sqrt{S} - \frac{\dfrac{13S}{4} - 1}{4\sqrt{S}\,(S-1)\pi_2} \tag{B19}$$

The effect of the axial location of the center of gravity appears in these four equations and in equation (24) only as a coefficient of S, $2\left[\left(l_1^2 + l_2^2\right)/l^2\right]$. This factor is designated the center-of-gravity influence coefficient. Thus, equation (24) is a relatively weak function of the center-of-gravity location. The center-of-gravity influence coefficient varies from 4/4 to 13/4 as the center-of-gravity location varies from midway between the bearings to

an outboard quarter point $l_1/l = 5/4$. Figure 2 shows the variation of this coefficient with the center-of-gravity axial location.

Equation (24) can easily be applied to cases other than the four presented in this report. For quick estimates, however, the graphs of equation (B2) can be used for center-of-gravity axial locations with $1/2 \leq |l_1/l| < 3/4$, since figure 2 reveals that the influence coefficient does not change greatly in this region.

Equations (B15), (B17), and (B19) reveal that there is no solution for $S = 1$ for cases 2, 3, and 4. For case 1, however, all solutions exist.
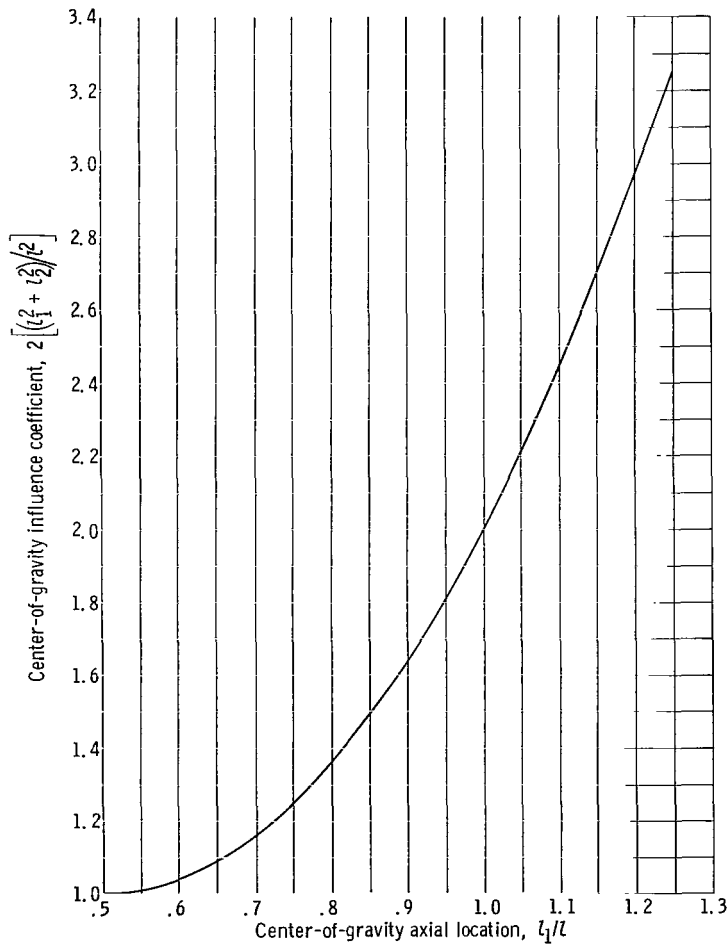

Figure 2. - Variation in center-of-gravity influence coefficient with center-of-gravity axial location.

DISCUSSION AND RESULTS

Universal Plots

The basic graphs of this report are the universal plots. They apply to a wide range of geometry and speed. The universal plots are made from equations (B2), (B15), (B17), and (B19).

Appendix B shows that a single two-branch curve can represent all geometries and speeds for case 1 in which the center of gravity is midway between the bearings. This abbreviated universal plot (made from eq. (B4)), shown in figure 3, has the adjusted shape-speed parameter

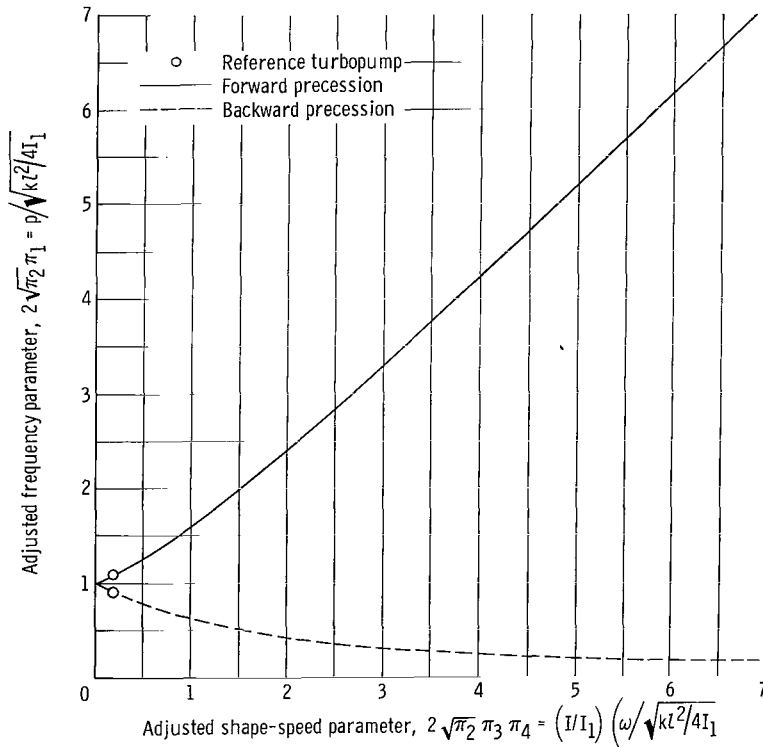$$\frac{I}{I_1} \frac{\omega}{\sqrt{\dfrac{k\ell^2}{4I_1}}}$$

Figure 3. - Abbreviated universal plot for center of gravity midway between bearings, case 1; equation (B4).

as the abscissa and the adjusted-frequency parameter

$$\frac{p}{\sqrt{\dfrac{k\mathit{l}^2}{4I_1}}}$$

as the ordinate. The upper branch in figure 3 represents forward precession, and the lower branch, backward precession. When $\delta = 1$, positive values of $\pi_3\pi_4$ in equation (B4) result from positive values of π_1 to yield the upper curve in figure 3. When $\delta = -1$, positive values of $\pi_3\pi_4$ result from negative values of π_1 to yield the lower curve. In reference 8, Den Hartog observed, presumably from experiment, that the low-frequency branch represents backward precession.

The backward-precession branch should be shown in the fourth quadrant, since it represents a direction opposite from the upper branch. Both branches are shown in the first quadrant to save space, however. Figure 3 displays only one-half of the total solution of equation (B4). Although not shown, a mirror image of figure 3 in the second quadrant represents the other symmetrical half.

Because equation (16) is of the eighth order in p, there are four additional solutions for case 1. These four solutions are represented by

$$(k - Mp^2)(k - Mp^2) = 0 \tag{29}$$

This equation results from setting $\mathit{l}_1/\mathit{l} = 1/2$ which permits factoring $(k - Mp^2)$ from the first two rows of the matrix in equation (15). Each factor in equation (29) yields

$$\frac{p}{\sqrt{\dfrac{k}{M}}} = \pm 1 \tag{30}$$

Yamamoto states in reference 2 that the precession frequency is constant when the center of gravity is midway between the bearings. His constant value is represented by equation (30), which, as discussed previously, represents only the less-interesting half of the eight solutions. Yamamoto's presentation in reference 2 therefore neglects the variable solutions of figure 3 and equation (B2) of this report.

For the axial turbopump studied in reference 6, the product

$$\frac{I}{I_1} \frac{\omega}{\sqrt{\dfrac{k\ell^2}{4I_1}}}$$

is 0.19 at design speed. This value for the abscissa in figure 3 locates the reference turbopump design operating point shown by the open circles.

When the center of gravity does not lie midway between the bearings, the universal plots consist of a family of curves with π_2 as the parameter. Figure 4 presents univer-
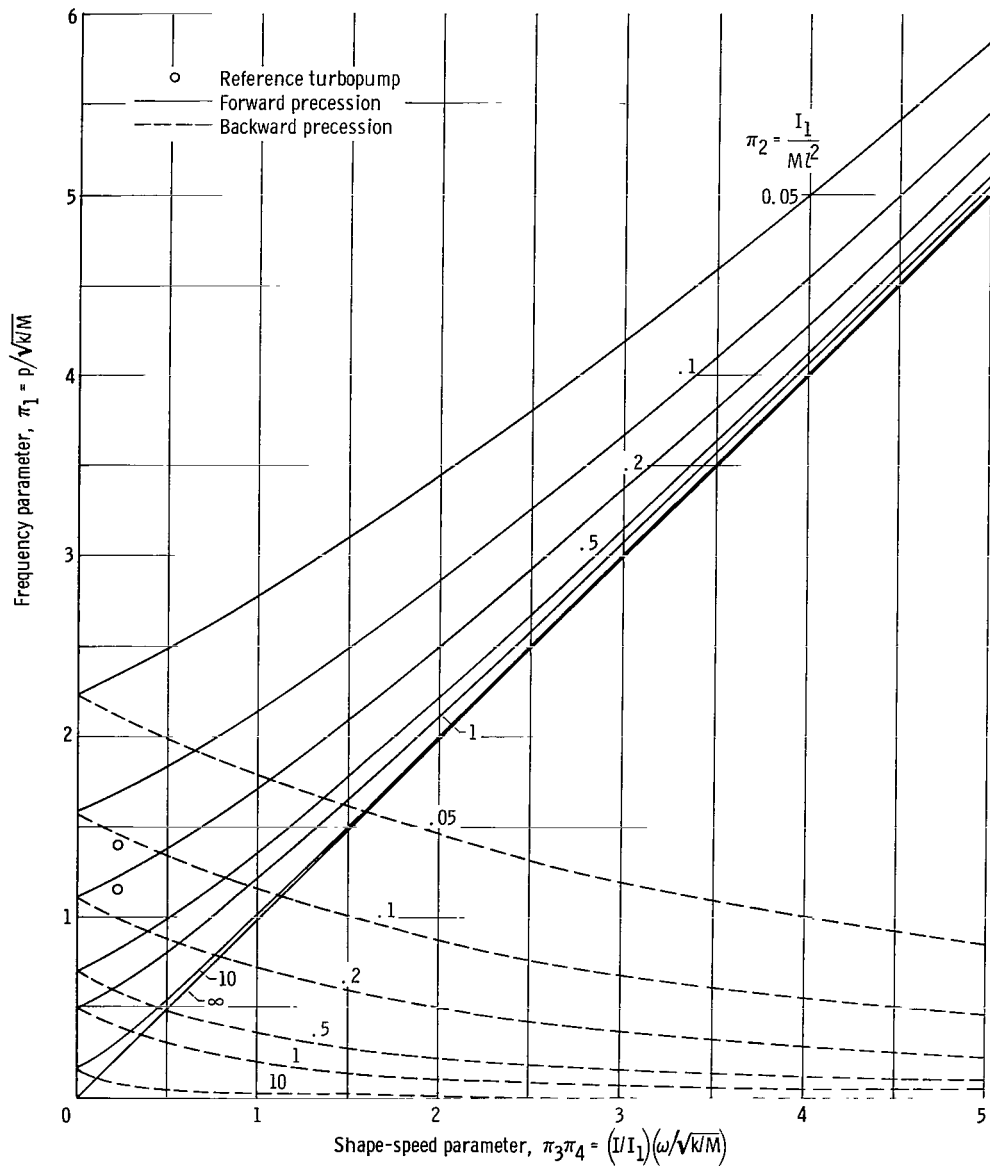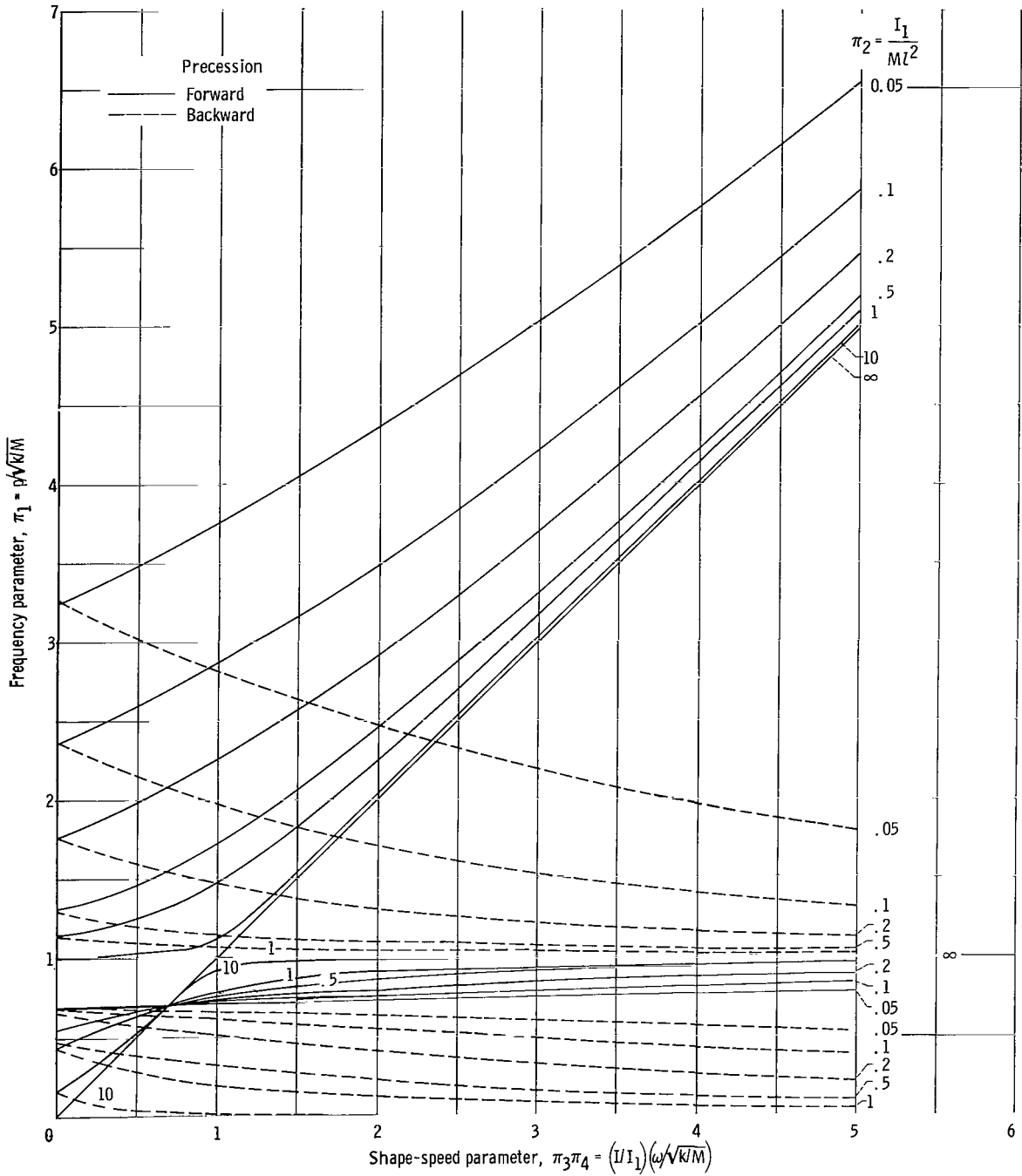

(a) Center of gravity midway between bearings; case 1; equation (B2).

Figure 4. - Universal plots.
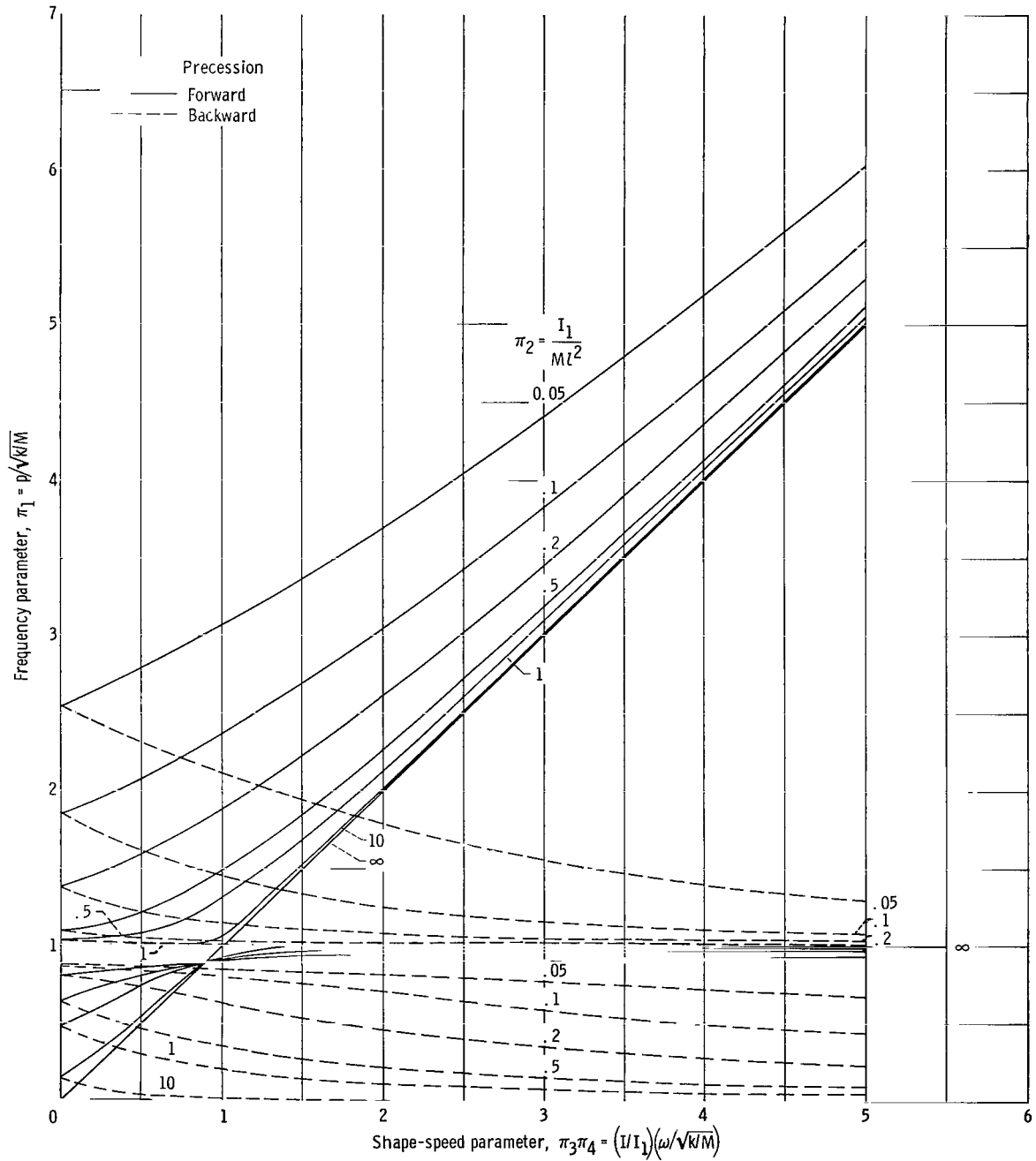
(b) Center of gravity at quarter point; case 2; equation (B15).

Figure 4. - Continued.

(c) Center of gravity at one bearing; case 3; equation (B17).

Figure 4. - Continued.

(d) Center of gravity at outboard quarter point; case 4; equation (B19).

Figure 4. - Concluded.

17

sal plots of this type for all four cases. In these figures the shape-speed parameter

$$\frac{I}{I_1} \frac{\omega}{\sqrt{\dfrac{k}{M}}}$$

is the abscissa, and the ordinate is the frequency parameter

$$\frac{p}{\sqrt{\dfrac{k}{M}}}$$

Figure 4(a) repeats the information for case 1, presented more concisely in figure 3, to provide a direct comparison of case 1 with the other three cases, as represented in figures 4(b) to (d). It is not possible to reduce the family of curves to one two-branch curve for cases 2 to 4. It may be of interest to note that the set of curves in figure 3 corresponds to the set in figure 4(a) (not shown) for $\pi_2 = 0.25$. This fact results from equating the corresponding ordinate or abscissa parameters $(2\sqrt{\pi_2}\,\pi_1 = \pi_1)$.

Figures 4(b) to (d) each present two forward-precession solutions (solid curves) and two backward (dashed curves). These four solutions plus their mirror images in the second quadrant (not shown in fig. 4) make up the eight solutions called for by equation (16).

Intersections of the curves with the ordinate axis of the universal plots represent vibration frequencies of nonrotating rotors. There is no distinction between forward and backward precession at these points, as the two branches of the curves join there. The solution given by equation (30) is of a different mode from the zero-speed solutions given in figure 4(a) by the ordinate-axis intersections.

The universal plots in figures 4(b) to (d) display the no-solution condition of equation (24) when $p/\sqrt{k/M}$ is plus or minus 1. A no-solution barrier does not exist, of course, for case 1, as shown in figure 4(a). For cases 2, 3, and 4, the no-solution barriers divide the plots into a low-frequency set and a high-frequency set. There is a forward- and a backward-precession branch in each set.

As rotor shapes become more disk-like and the disk effect π_2 approaches infinity, curves on the universal plots approach a 45° line through the origin for all four cases. This condition is obvious from equation (23). It occurs both below and above the no-solution barrier of figures 4(b) to (d). In fact, equation (23) also shows that the no-solution barrier itself $(\pi_1 = 1)$ also represents geometries in which π_2 is infinite.

In figures 4(b) to (d), forward precession curves in the low-frequency set all cut the

45° line through the origin in a common point. This observation can be shown analytically by setting

$$\delta = 1$$

and

$$\pi_3 \pi_4 = \sqrt{S} = \pi_1$$

in equation (24). The result is

$$\pi_1 = \frac{p}{\sqrt{\dfrac{k}{M}}} = \frac{1}{\sqrt{2\left(\dfrac{\imath_1^2 + \imath_2^2}{\imath^2}\right)}} \tag{31}$$

which is independent of π_2.

Comparison of the universal plots in figure 4 reveals that, for a given shape and rotational speed, the effect of the center-of-gravity axial location as it is displaced outward from the midway point is a small rise in the magnitude of precession frequency.

Frequency Plots

Curves of precession frequency plotted against rotational frequency are helpful in visualizing the locations of critical speed for a given geometry. Figure 5 presents a few frequency plots for selected geometries of cases 1 and 3. Less general than the universal plots, the frequency plots are obtainable from them or from equations (B4) and (24) by specifying π_3. When π_3 is 1, frequency plots and universal plots are identical.

Each curve in figure 5 denoting constant π_3 represents a constant geometry. The design operating point of the reference turbopump is shown by the two lowest open circles in figure 5(a). The straight lines in figure 5 denote various critical speeds, to be discussed in the following two sections. Thus, each curve in figure 5 traces the passage of a given machine through potential critical speeds as it accelerates or decelerates.
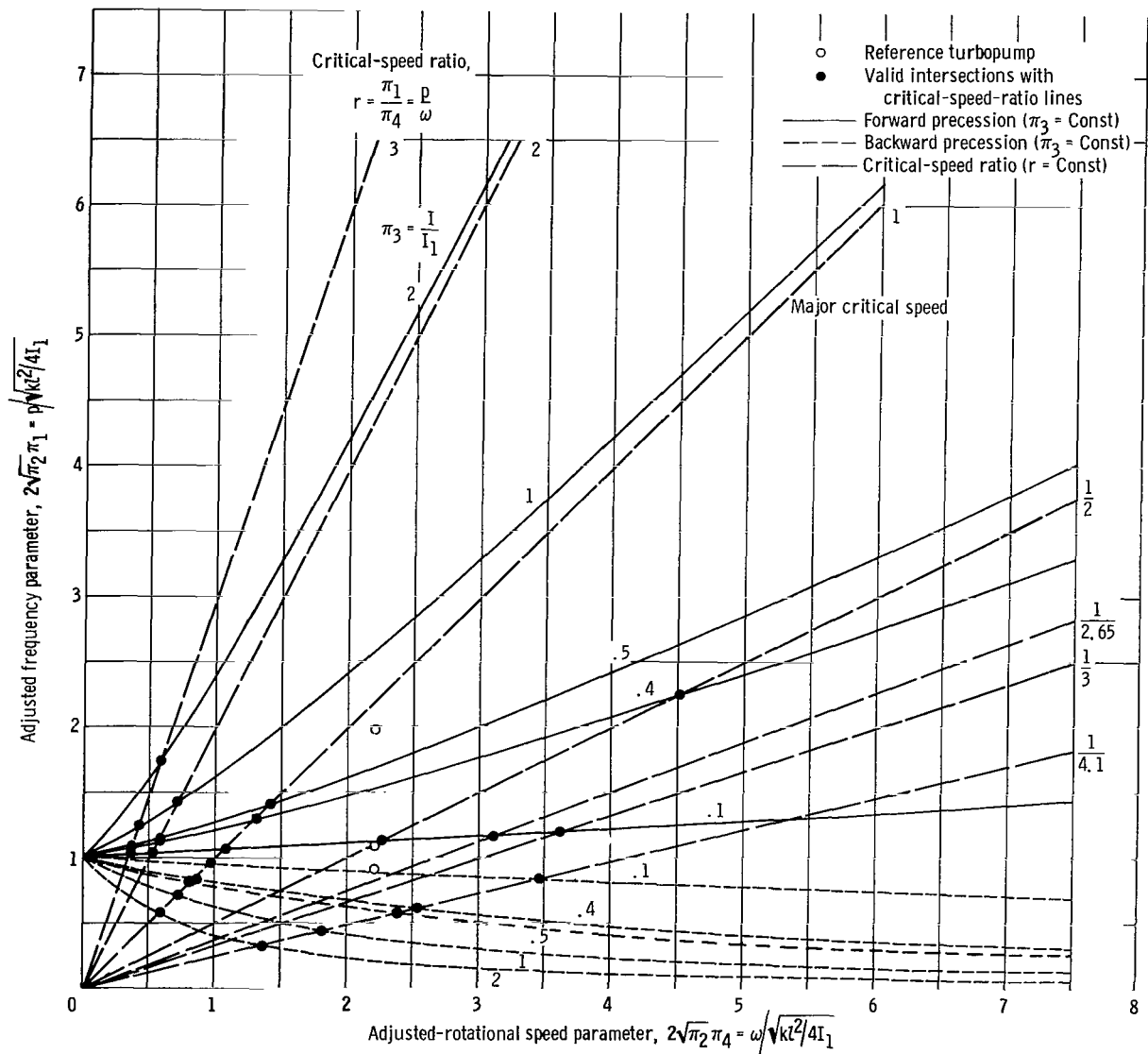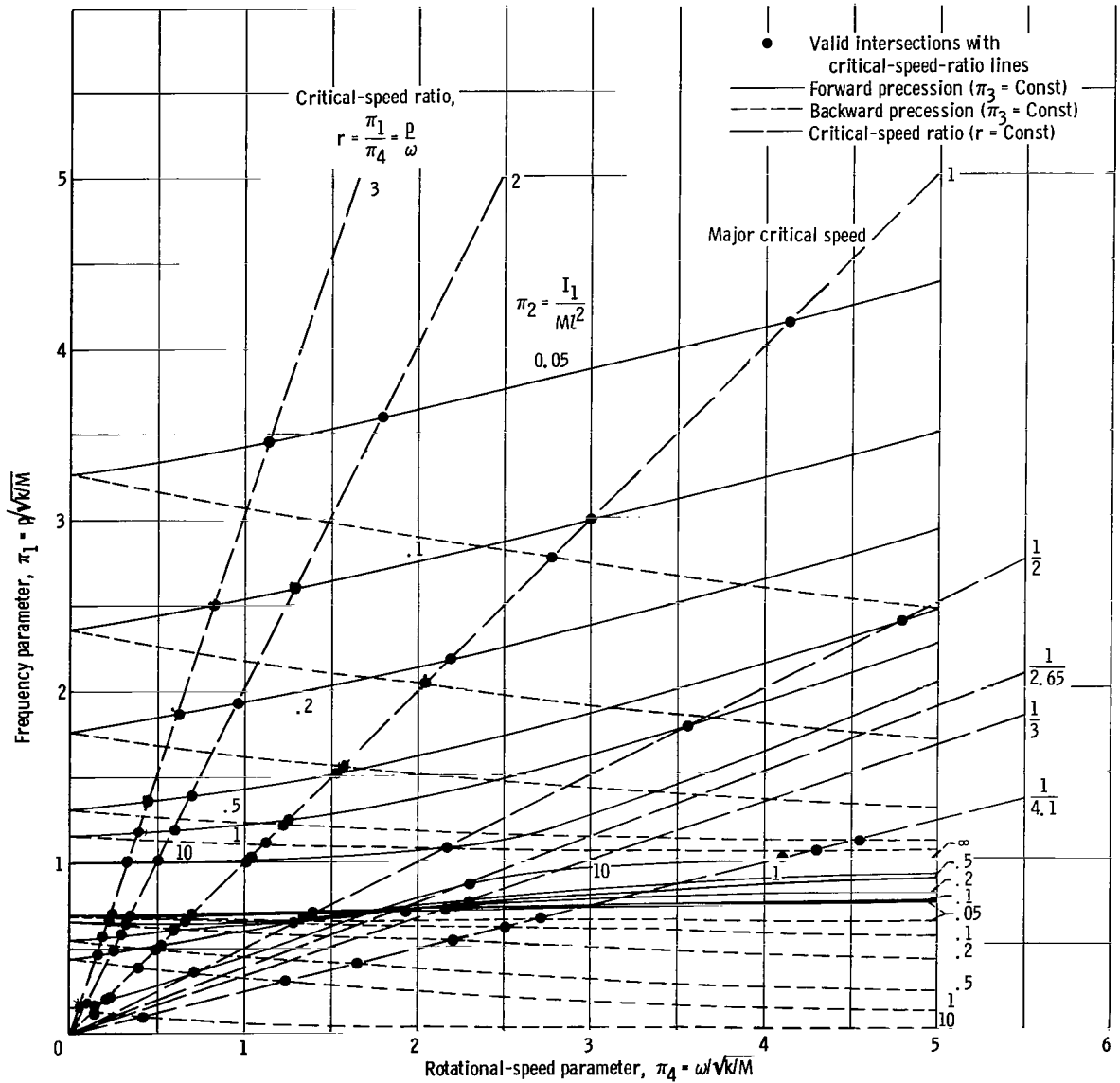
(a) Center of gravity midway between bearings; case 1.

Figure 5. – Frequency plots showing critical speeds.
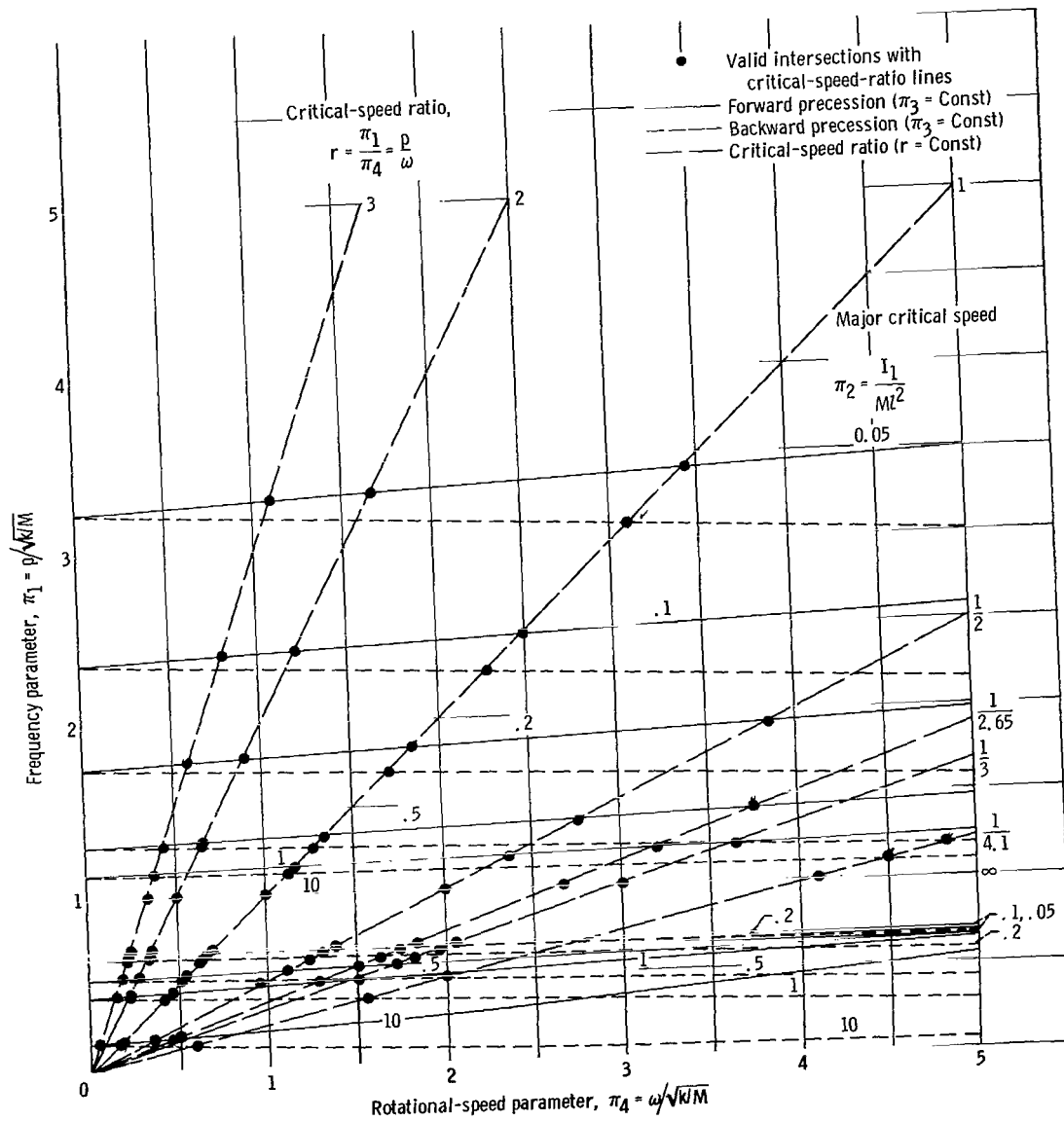
(b) Center of gravity at one bearing; case 3; $\pi_3 = I/I_1 = 0.1$.

Figure 5. - Continued.

(c) Center of gravity at one bearing; case 3; $\pi_3 = I/I_1 = 0.4$.

Figure 5. - Continued.

Critical-speed ratio,
$$r = \frac{\pi_1}{\pi_4} = \frac{p}{\omega}$$

● Valid intersection with critical-speed-ratio lines
——— Forward precession (π_3 = Const)
- - - Backward precession (π_3 = Const)
— — Critical-speed ratio (r = Const)

Major critical speed

$$\pi_2 = \frac{I_1}{Ml^2}$$

Frequency parameter, $\pi_1 = p\sqrt{k/M}$

Rotational-speed parameter, $\pi_4 = \omega\sqrt{k/M}$
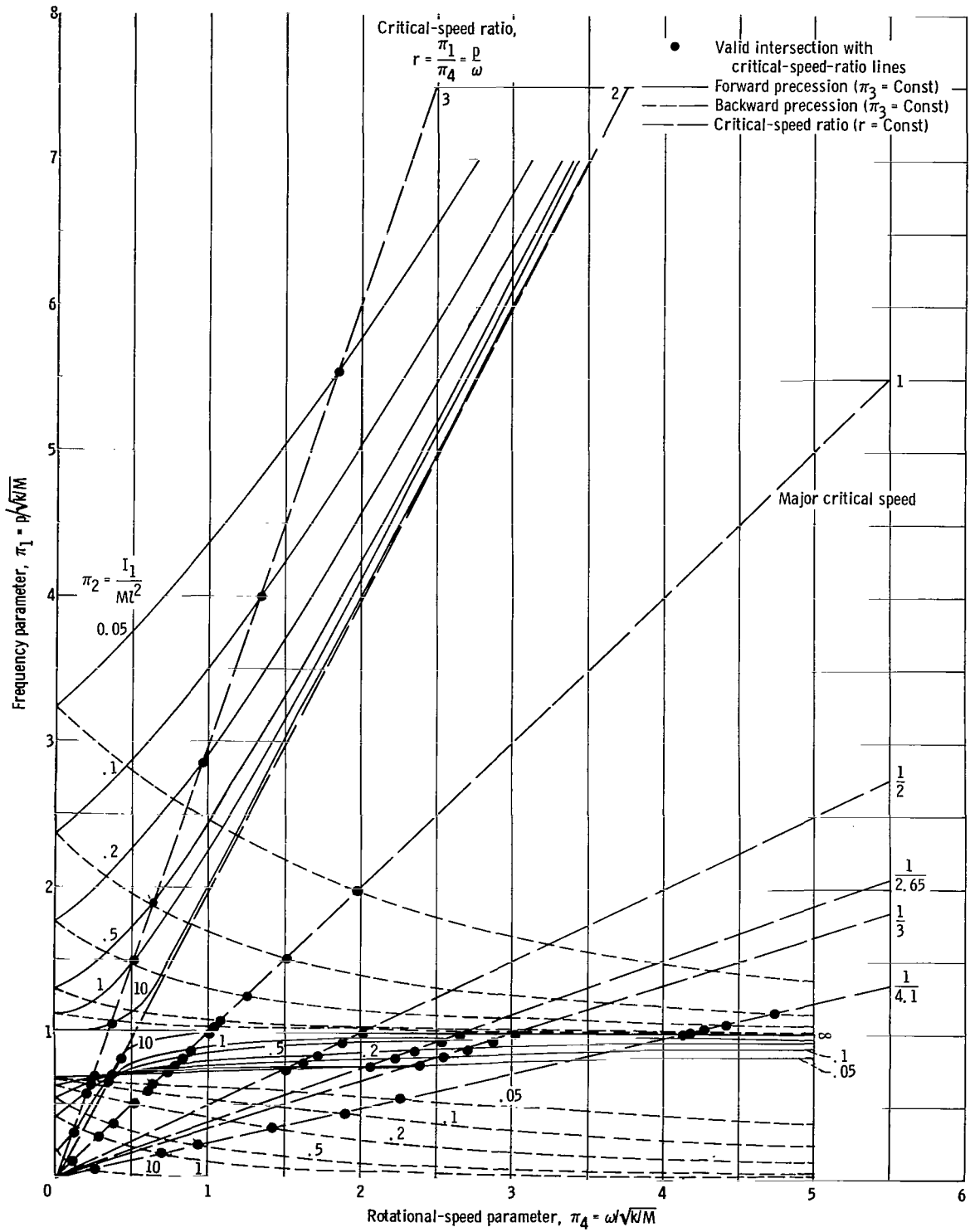
(d) Center of gravity at one bearing; case 3; $\pi_3 = I/I_1 = 2$.

Figure 5. - Concluded.

Major Critical Speeds

An important aspect of this investigation is to locate the major critical speeds for all geometries considered. This information is significant because forward-precession major critical speeds may be excited by rotor unbalance. For this purpose, plots relating major critical speed with geometry are helpful. Major critical speed plots, presented in figures 6 and 7, are derived from equation (28). They may also be obtained from intersections of the curves on the universal plots with straight lines through the origin having slopes of $1/\pi_3 = I_1/I$.

The abbreviated major critical-speed plot for case 1 consists of one two-branch curve and is shown in figure 6. The abscissa in this figure is I/I_1, and the ordinate is

$$ 2\sqrt{\frac{I_1}{M\ell^2}} \; \frac{\omega_{cr}}{\sqrt{\frac{k}{M}}} $$

The curves in figure 6 are derived from equation (B9). The upper branch of the curve gives the solution for forward precession; the lower branch is for backward precession.
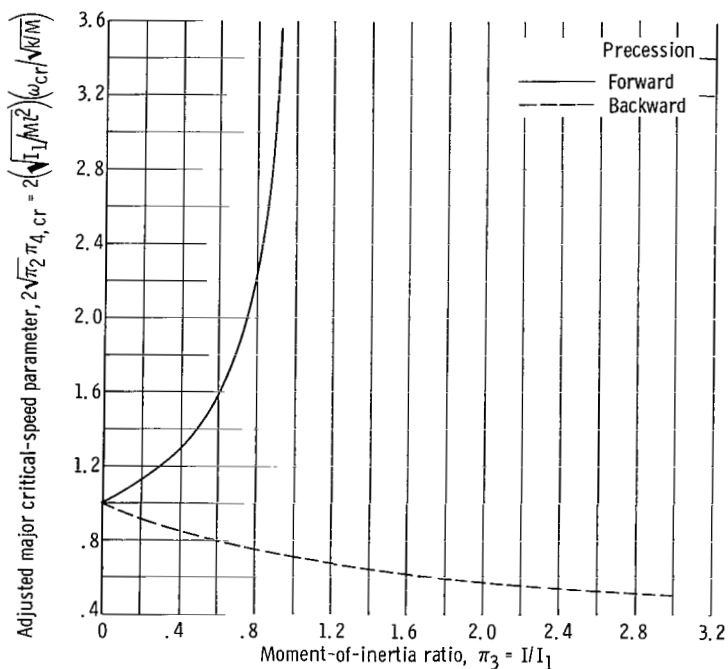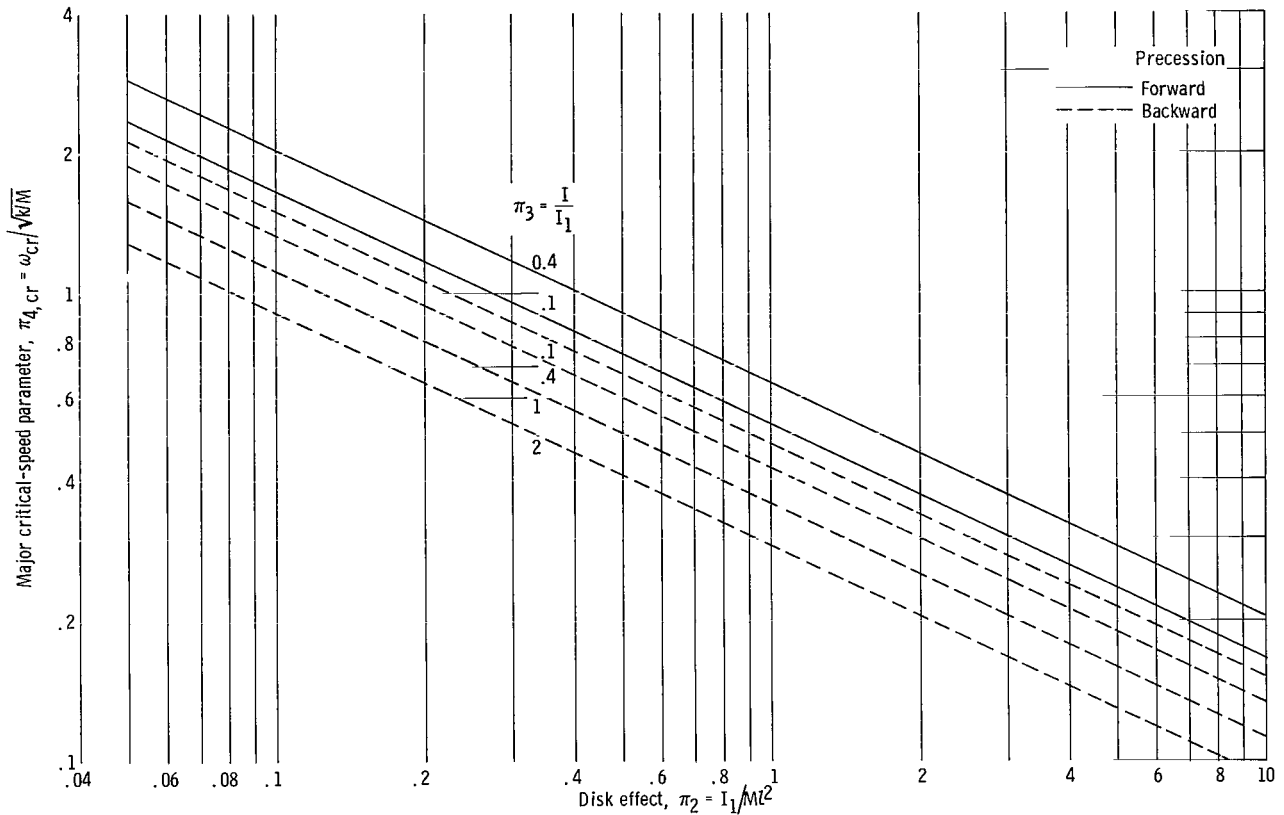

Figure 6. - Abbreviated major critical-speed plot for center of gravity midway between bearings, case 1; equation (B9).

(a) Center of gravity midway between bearings; case 1.

Figure 7. - Major critical-speed plots.

Thus, for case 1, major critical speeds, when they occur, are higher for forward than backward precession for any shape. Equation (B9) and figure 6 show that, for constant π_3 for case 1, the major critical speed is inversely proportional to $\sqrt{\pi_2}$.

Equation (B9) shows that, for forward precession ($\delta = 1$), the major critical speed becomes infinite when π_3 is 1 and is imaginary beyond 1. The upper curve in figure 6 illustrates these conditions. This fact implies that forward major critical speed can be avoided entirely for case 1 by using designs having I/I_1 greater than 1. If such designs are not feasible, designing with I/I_1 as close to 1 as possible may yield a major critical speed well above the design speed.

Because the dashed curve in figure 6 remains finite, backward-precession major critical speeds cannot be so easily avoided by selective design. However, if designs with a low value of π_2 (pencil shapes) are used, the major critical speed may be high enough to exceed design speed.

The steep slope of the upper curve in figure 6 reveals that the major critical speed of forward precession is very sensitive to shape. The dashed curve shows that the major
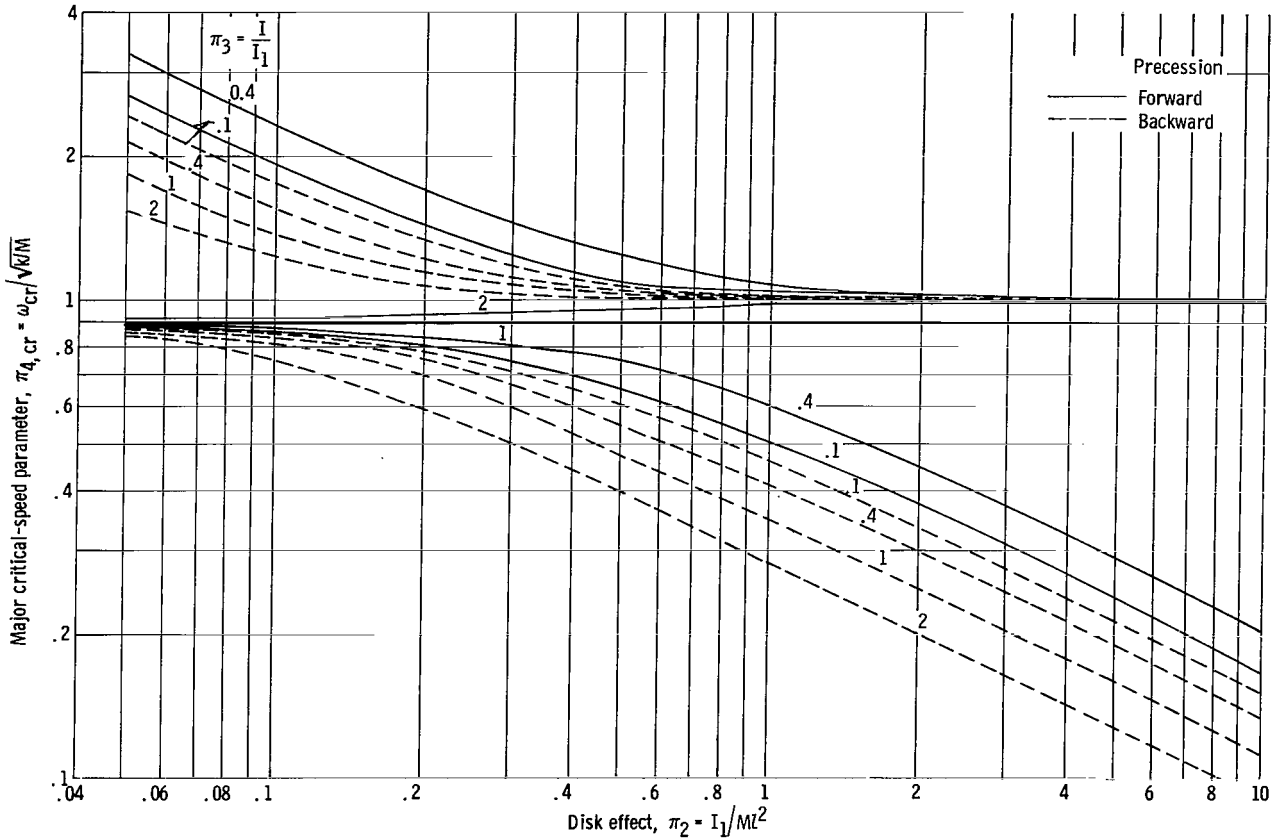
(b) Center of gravity at quarter point; case 2.

Figure 7. - Continued.

critical speed of backward precession is much less sensitive. Also, the adjusted major critical-speed parameter for backward precession decreases with increasing I/I_1.

According to the locations of the lowest two open circles in figure 5(a), the axial turbopump of reference 6 passes through a major critical speed as it accelerates to the design point. Major critical-speed plots for all four cases are shown in figure 7. These figures have I_1/Ml^2 as the abscissa and $\omega_{cr}/\sqrt{k/M}$ as the ordinate, with I/I_1 as a parameter. Figure 7(a), which repeats the information given in figure 6, aids in a comparison. As in the universal plots, there are two families of curves on the major critical-speed plots of cases 2 to 4. One family is above the no-solution condition, and one is below. As noted earlier, the positive sign before the radical in equation (28) yields the high-frequency set. The curves in figure 7 show that, in general, major critical speed decreases as I_1/Ml^2 increases. For cases 2 to 4, figures 7(b) to (d) show an exception to this observation for low-frequency forward precession when I/I_1 is greater than 1. When I/I_1 is 1, the forward major critical speed is independent of I_1/Ml^2 for cases 2 to 4. This observation arises from setting $\delta = 1$, $\pi_1 = \pi_4$, and $\pi_3 = 1$ in equation (23). The
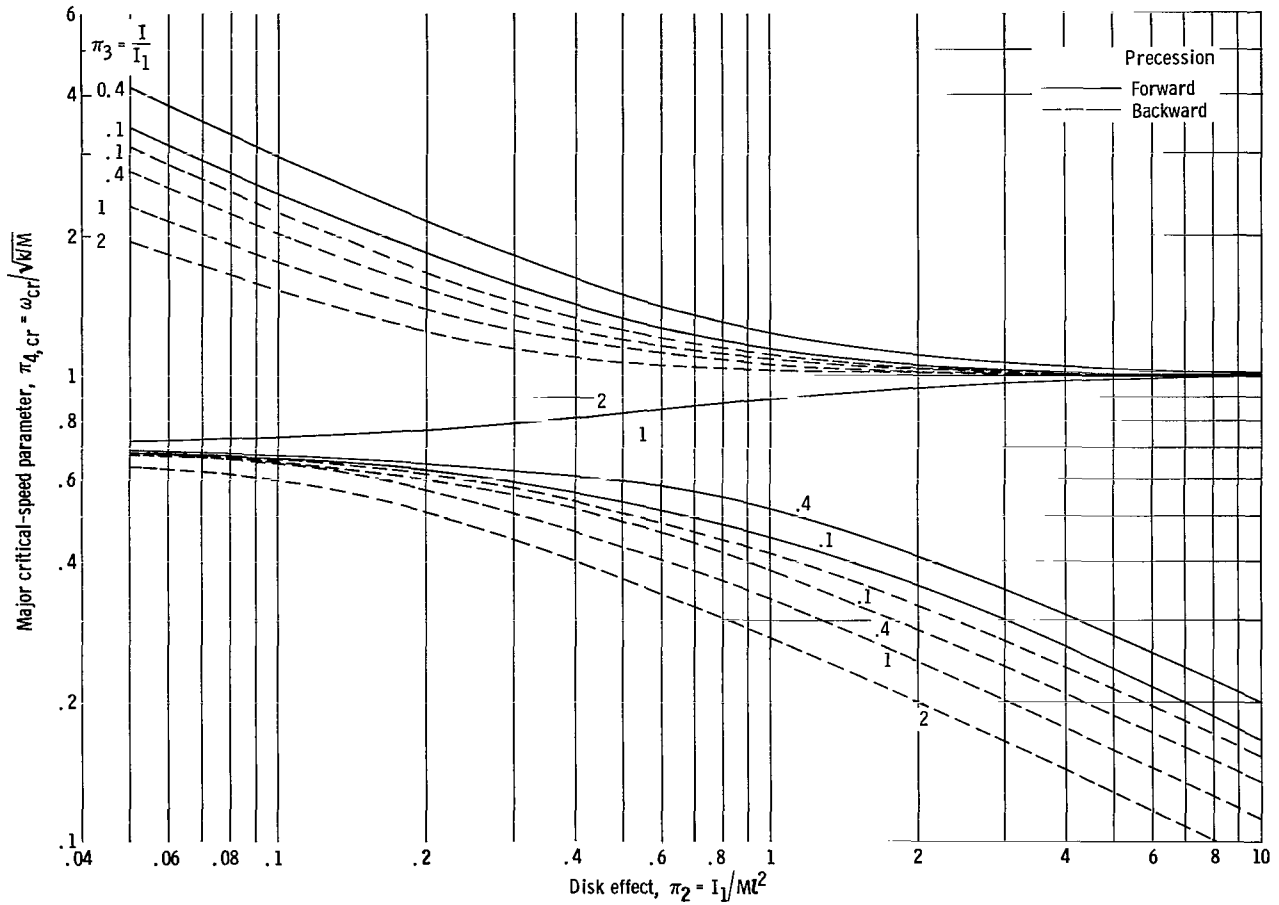
(c) Center of gravity at one bearing; case 3.

Figure 7. - Continued.

result is again equation (30), which was derived earlier for a different situation.

On the other hand, for forward precession, major critical speed increases as I/I_1 increases. The opposite variation occurs for backward precession. Thus, for backward precession, disks have lower major critical speeds than pencil-shape configurations. No such conclusive statement can be made for forward precession because of the opposite effects of I_1/Ml^2 and I/I_1.

At values of I_1/Ml^2 greater than about 1, its effect on major critical speed is negligible for the high-frequency set. Furthermore, in this range of I_1/Ml^2, variations in I/I_1 have a minor effect as the curves for this set converge.

It was observed for case 1 from equation (B9) and in figure 6 that no major critical speed exists for forward precession when I/I_1 is 1 or higher. This observation is true for the other three cases, too, but only for forward precession in the high-frequency set. Equation (28) is useful in explaining this circumstance. When $\delta = 1$ and $\pi_3 = 1$, it is
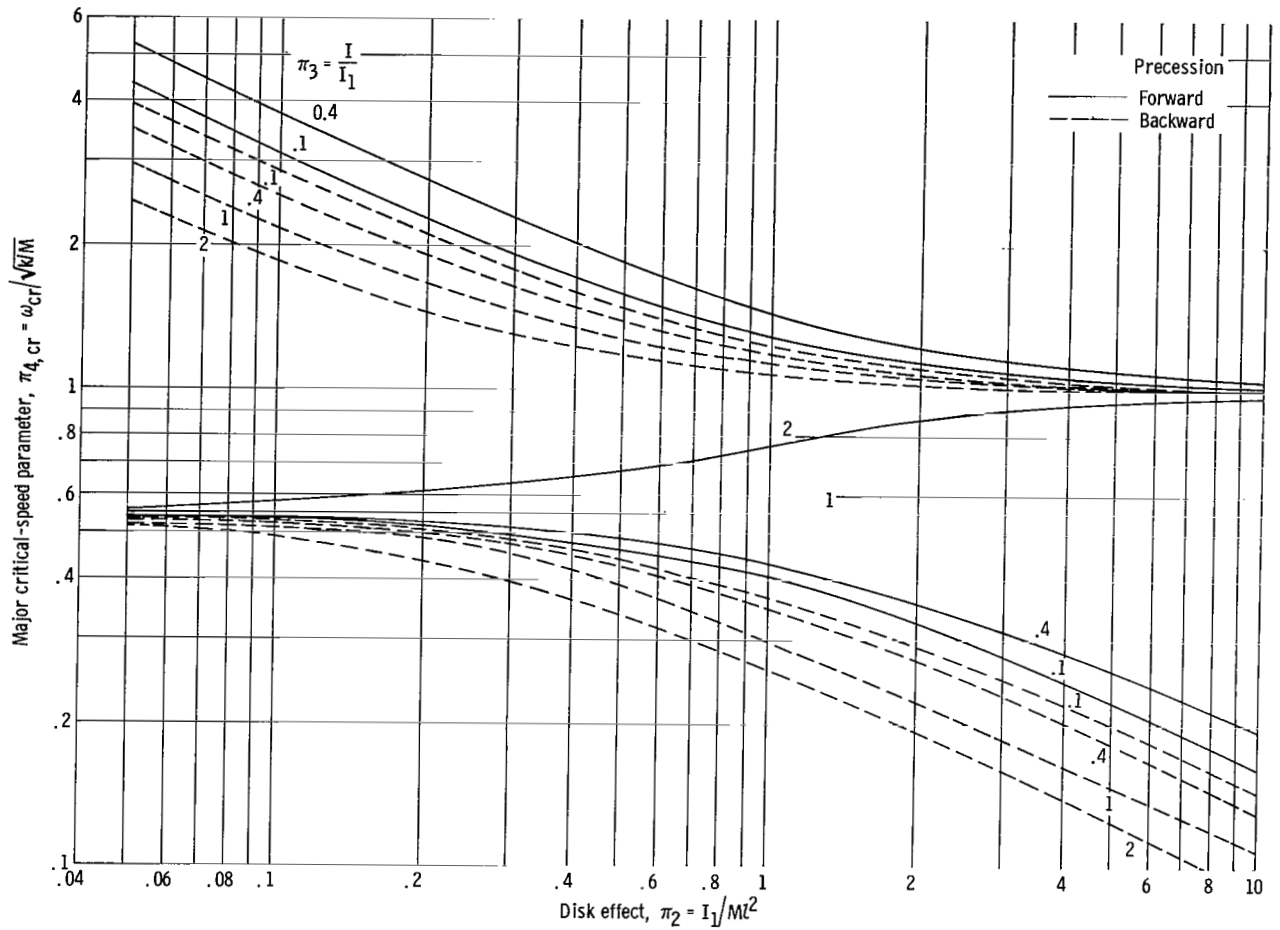
(d) Center of gravity at outboard quarter point; case 4.

Figure 7. - Concluded.

evident from equation (28) that $\omega_{cr}/\sqrt{k/M}$ becomes infinite. When $\delta = 1$ and $\pi_3 > 1$, the magnitude of the expression following the $\pm$ sign exceeds that preceding it. Therefore, $\omega_{cr}/\sqrt{k/M}$ from equation (28) is imaginary when the minus sign is used; this condition pertains to the high-frequency set.

Consideration of the universal plots may give added insight to this explanation. A 45° line through the origin on a universal plot not only locates the major critical speeds for an I/I_1 of 1, but also represents a value of infinity for $I_1/M\ell^2$. This condition is also evident from equation (24) when π_2 is infinite. The forward-precession curves of the high-frequency set therefore cannot intersect the 45° line when I/I_1 is 1. Thus, no major critical speeds are possible for forward precession of the high-frequency set when I/I_1 is 1 or greater. Figures 3 and 4(b) to (d) all confirm this observation. It is apparent, however, that intersections with the forward-precession low-frequency curves still occur.

Figure 8 presents the major critical-speed results in a form to show the effect of

28

(a) $\pi_3 = I/I_1 = 0.1$.

Figure 8. – Effect of center-of-gravity location on major critical speed.

29
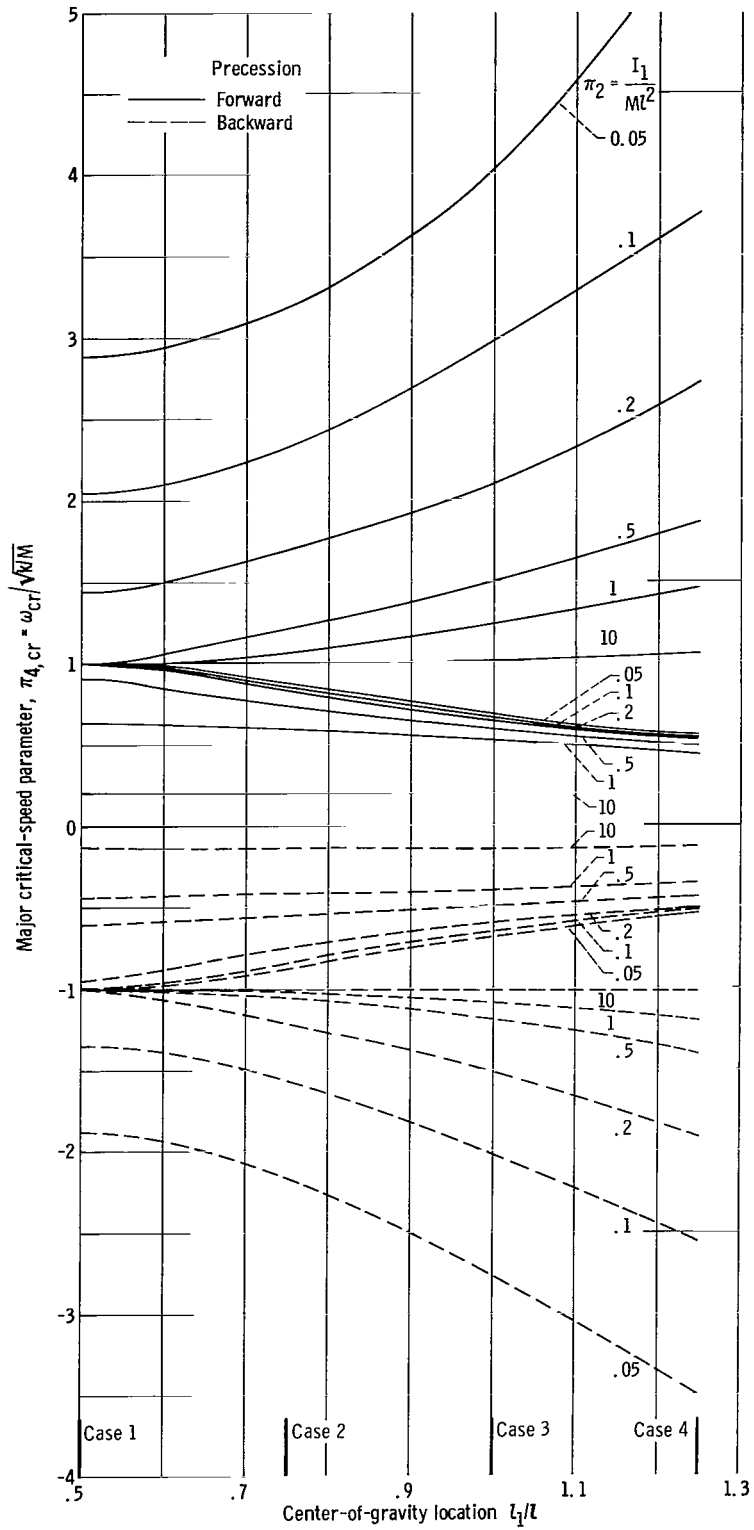
(b) $\pi_3 = I/I_1 = 0.4$.

Figure 8. - Continued.
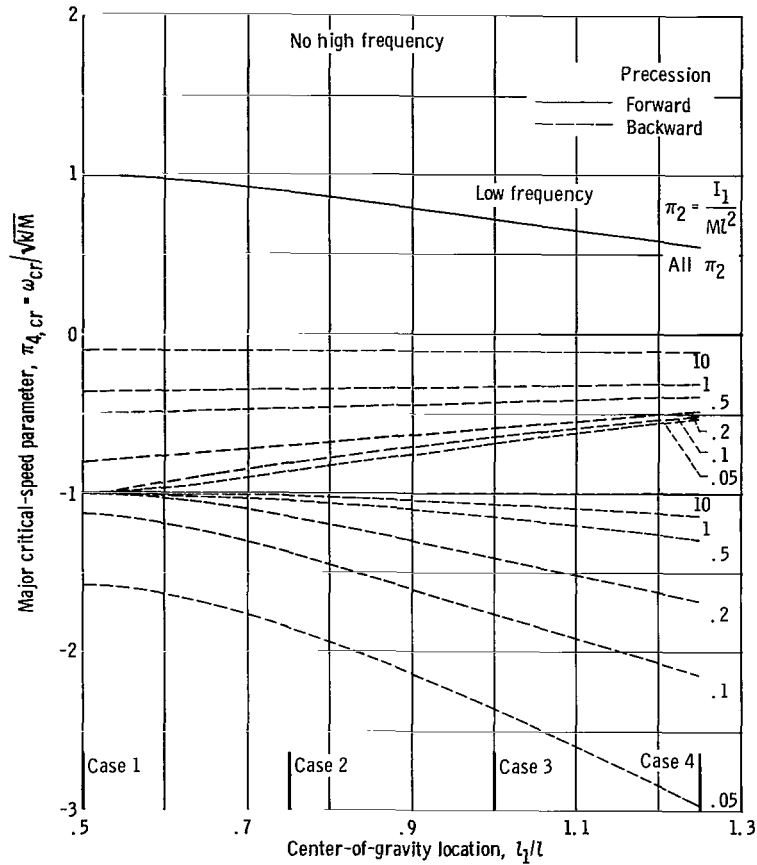
(c) $\pi_3 = I/I_1 = 1$.

Figure 8. - Continued.

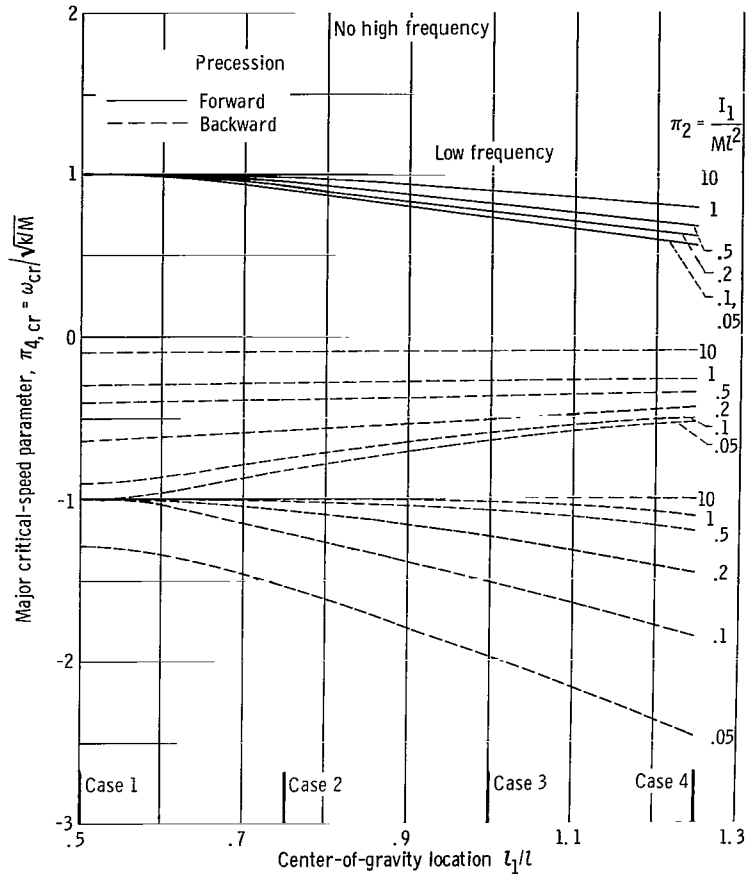axial location of the center of gravity. Four plots are presented in figure 8, each for a selected value of I/I_1. In addition, $I_1/M\ell^2$ varies as a parameter on each plot. The plots in figure 8 are derived directly from the corresponding plots of figure 7 or from equation (28).

To avoid confusion among the many curves, the backward-precession curves in figure 8 are shown in the fourth quadrant. As usual, they are dashed. Figure 8 has a mirror image in the second and third quadrants. The abscissa range of ℓ_1/ℓ of the image is from -0. 25 to 0. 5; that is, ℓ_2/ℓ varies from 0. 5 to 1. 25.

There are two families of curves for both forward and backward precession except for ℓ_1/ℓ of 0. 5, as noted in the discussion of figure 4. The merging curves in figure 8 graphically illustrate the fact discussed in connection with figure 3 that the two sets of solutions ostensibly absent for case 1 actually exist in $\pi_1 = 1$. The slopes of all the curves in figure 8 are zero at the bearing centerline midpoint because of symmetry. Differentiating equation (28) and using $\ell_1/\ell = 1/2$ proves this observation mathematically.

31

(d) $\pi_3 = I/I_1 = 2$.

Figure 8. - Concluded.

Figure 8 shows that the effect of the axial location of the center of gravity decreases as both π_2 and π_3 increase. Therefore, the effect of the axial center-of-gravity location decreases as geometries become more disk-like.

Furthermore, there are no forward precession high-frequency curves in figures 8(c) and (d) for reasons mentioned on pages 27 and 28.

In figure 8, solutions that lie within the -1 to 1 ordinate band reveal a trend of decreasing major critical-speed magnitude as the center of gravity is located progressively outward from the bearing centerline midpoint. Both families outside this band display the opposite trend.

In figure 8(c), in which $\pi_3 = 1$, the forward-precession low-frequency curves are identical for all values of π_2. This characteristic, observed in figures 7(b) to (d), results from equation (31).

Figures 7 and 8 should aid in preliminary design by pointing out potential major critical speeds for various configurations.

Nonsynchronous Critical Speeds

It is well known that critical speeds other than the major critical speed may induce destructive vibrations. The accompanying motions of the rotor are commonly called nonsynchronous precessions.

Yamamoto has made the most thorough investigation of nonsynchronous precessions in rotors supported by ball bearings. He has determined that the bearings are responsible for this phenomenon. In reference 2, he reports that two classes of nonsynchronous critical speeds occur when double-row self-alining ball bearings are used. These motions occur at rotor speeds both greater and less than synchronous critical. The spring characteristics are linear for this bearing type. Therefore, the rotors studied herein may be assumed to be mounted in double-row ball bearings because of the linear spring constant used in this analysis.

Yamamoto's work in reference 3 reveals two other classes of nonsynchronous critical speed for single-row ball-bearing configurations. These motions all occur at rotor rotational speeds above synchronous. This type of bearing has nonlinear and nonsymmetrical spring characteristics because of the absence of self alinement in the bearings.

Therefore, the conditions for nonsynchronous critical speeds resulting from single-row ball-bearing defects cannot be rigorously applied to the solutions of the present analysis. However, even for double-row ball-bearing defects, the present analysis is approximate because of its idealized assumption of no damping. Furthermore, Yamamoto shows in reference 3 that theoretical solutions from his linear spring-constant analysis are good approximations to his experimental results obtained with single-row ball bearings (nonlinear spring constants). Therefore, nonlinear spring constant conditions are applied herein without hesitation to the present analysis for the purpose of locating potential nonsynchronous critical speeds.

Double-row ball bearings. - In experiments with self-alining ball bearings, Yamamoto observed that very slight defects can produce driving forces at frequencies different from the shaft speed. One class of such nonsynchronous motion arises from nonuniformity in the ball diameters. Another set of nonsynchronous precession may result from noncircular inner or outer bearing races. Yamamoto observed that all commercial bearings made in Japan, and presumably elsewhere, have these defects.

Nonuniform ball diameters cause nonsynchronous precession at rotor speeds higher than critical. Yamamoto's work disclosed that the most serious conditions of this type occur when the critical-speed ratio is

$$r = \frac{p}{\omega} = \frac{1}{2.65} \tag{B10}$$

for forward precession. The constant in this expression is an average value obtained experimentally and theoretically by Yamamoto, and reported in references 2 and 9. He presents the following relation in these references:

$$r = \frac{1}{2 + 2\frac{d}{\mathscr{D}}} \tag{32}$$

For backward precession, Yamamoto finds

$$r = \frac{p}{\omega} = -\frac{1}{4.1} \tag{B11}$$

Appendix B uses these expressions in equation (B8) for case 1 yielding equations (B12) and (B13). These equations are plotted in figure 9, which is a companion plot of figure 6, with appropriate change of constant. Figure 9 shows that forward nonsynchronous precession of this type cannot occur for shapes having I/I_1 greater than the critical-speed ratio $1/2.65$. Thus, forward-precession nonsynchronous speeds of this type are limited to a small range of π_3. Backward precession is possible over the entire range of I/I_1, however.

At this point, the use of equation (B8) is convenient in making a general statement:

$$2\sqrt{\pi_2}\,\pi_4 = \frac{1}{\sqrt{r(r - \delta\pi_3)}} \tag{B8}$$

For case 1, no forward-precession critical speeds (either synchronous or nonsynchronous) exist when the moment-of-inertia ratio π_3 equals or exceeds the critical-speed ratio r.

Yamamoto's work revealed that the amplitudes during backward-nonsynchronous motion are smaller than in forward precession. Therefore, although the dashed curve remains finite in figure 9, the small amplitudes reduce the severity of the consequences of this motion.

Lines representing $r = 1/2.65$ and $r = 1/4.1$ for case 1 are shown in the frequency plot of figure 5(a). Likewise, corresponding lines are shown in the frequency plots of figures 5(b) to (d) for case 3.

In figure 5, only the intersections of the $r = 1/2.65$ lines with the forward-precession curves are meaningful. Similarly, the meaningful intersections for the $r = 1/4.1$ lines are with the backward-precession curves. Solid circles in figure 5 denote valid intersections.
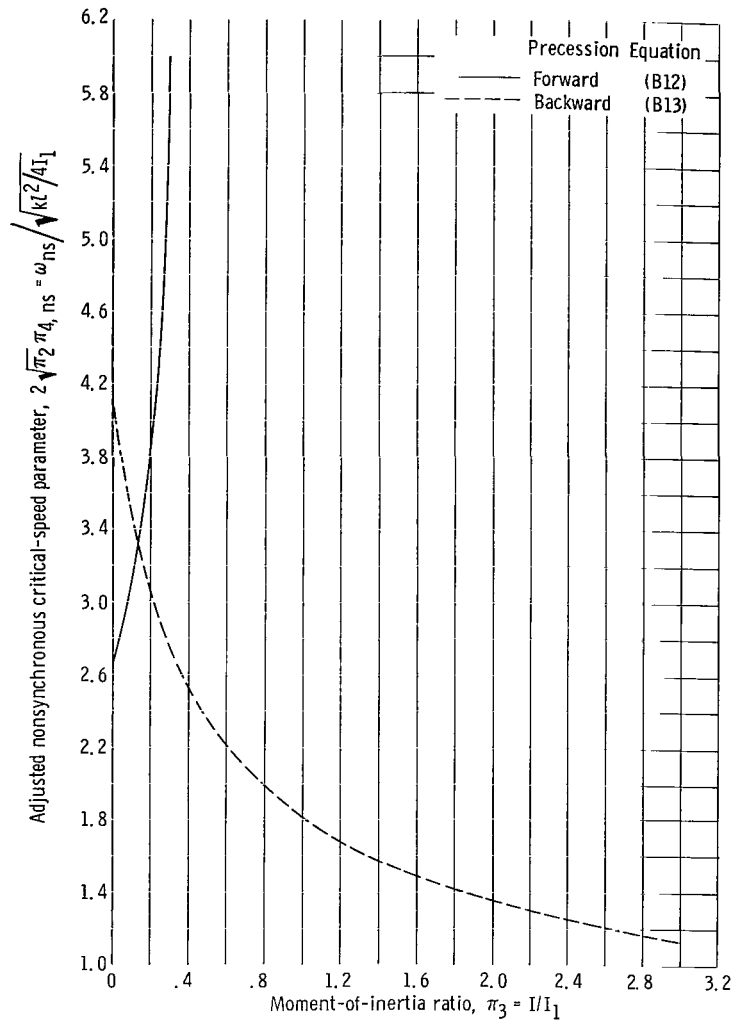
34

Figure 9. - Abbreviated nonsynchronous critical-speed plot for
r = 1/2.65 and r = -1/4.1 for center of gravity midway
between bearings; case 1, equations (B12) and (B13).

Most of the r = 1/2.65 and r = 1/4.1 intersections in figures 5(b) to (d) occur below the no-solution barrier $|p/\sqrt{(k/M)}|$ = 1 for both forward and backward precession. Although these intersections are at the lower end of the rotor-rotational-speed scale, they occur at more than twice the major critical speeds.

In reference 2, Yamamoto points out that noncircular inner and outer bearing races cause nonsynchronous forward precession at critical-speed ratios of 2, 3, and 5. The r = 5 motion is not serious, however, because of the low amplitudes he observed at this condition. Lines denoting critical-speed ratios of 2 and 3 are shown on the frequency plots of cases 1 and 3 in figure 5. All intersections, shown by solid circles, take place at rotor rotational speeds well below the major critical speeds. This observation im-

35

plies that even low-speed machines can experience this type of nonsynchronous precession. Furthermore, most machines, including the reference turbopump, must accelerate through these critical speeds to reach design speed.

Figure 5(d) shows that when I/I_1 is 2, no high-frequency forward-precession intersections exist with the $r = 2$ lines. This circumstance is analagous to that for case 1 in which it was noted that, by equation (B8), no forward precession exists when $\pi_3 \geq r$. For cases 2 to 4, both a graphical and a mathematical explanation aid in understanding the absence of forward-precision intersections when $\pi_3 = r = 2$.

Although not presented herein, frequency plots for cases 2 to 4 made for I/I_1 of 2 would also disclose no nonsynchronous critical speeds for the forward-precession high-frequency sets when $r = 2$. Consideration of the location of the $\pi_2 = \infty$ line on a frequency plot will illuminate this situation because no forward-precession high-frequency solutions are allowed below this line. For example, on a frequency plot constructed for $\pi_3 = 2$, the $\pi_2 = \infty$ line coincides with a critical-speed-ratio line of $r = 2$ and therefore allows no high-frequency solutions. More generally, coincidence of the $\pi_2 = \infty$ line and a critical-speed-ratio line for forward precession ($\delta = 1$) on a frequency plot for $\pi_3 = r$ can be proved mathematically from equation (23).

Therefore, a general conclusion can be stated for all cases. Forward-precession high-frequency critical speeds do not exist for geometries in which I/I_1 equals or exceeds the critical-speed ratio r. Figures 4 and 5 show that forward-precession low-frequency intersections exist, however.

It is unlikely that a set of bearings would have either nonuniform ball diameters or noncircular bearing races without having both defects. Thus, it may be assumed that all the critical speeds revealed for both kinds of bearing defect will occur.

Single-row ball bearings. - One class of nonsynchronous motion associated with single-row ball bearings is called subharmonic. Yamamoto observed this motion only in forward precession. Subharmonic motion is characterized by critical-speed ratios r of 1/2, 1/3, . . . 1/n, where n is a positive, real integer. It can occur only after the major critical speed is exceeded.

Lines for subharmonic motion are shown on the frequency plots for cases 1 and 3 in figure 5. Only intersections with forward-precession curves are valid, as shown by solid circles. Figure 5(a) shows that no high-frequency nonsynchronous precession of this type is possible for case 1 when I/I_1 is 0.5 or greater. This observation is also true for all cases, and is a consequence of the general conclusion stated earlier relating π_3 and r.

The axial turbopump studied in reference 6 was mounted in single-row ball bearings. According to figure 5(a), the locations of the two lowest open circles reveal that it passes through the $r = 1/2$ nonsynchronous critical speed when accelerating to the design point. In fact, the design point itself lies close to this nonsynchronous condition.

Yamamoto further observed that when single-row ball bearings are used, two natural frequencies build up together at certain speeds. The absolute value of their sum or difference is related to rotor rotational speed by

$$\omega = \left| p_i \pm p_j \right| \tag{33}$$

in which p_i and p_j are any two of the natural frequencies as calculated from equation (24). In reference 3, Yamamoto reports that vibration amplitudes from these sources may exceed those of the major critical speed. It is evident from any of the universal plots that the condition $i = j$ is not allowed, except for the trivial case of zero rotor rotational speed. In this instance, only

$$p_1 = p_4$$

and

$$p_2 = p_3$$

are allowed.

It was observed in figure 5(a) that there are only two solutions for case 1 for each value of I/I_1. The only summed-and-differential motion possible for this case is therefore

$$\omega = \left| p_1 - p_4 \right|$$

where p_1 represents forward-precession solutions, and p_4 represents backward-precession solutions.

The uppermost open circle in figure 5(a), obtained by adding the ordinates of the two lowest open circles, represents the summed-and-differential motion for the reference axial turbopump. The location of this circle relative to the 45° line through the origin shows that this turbopump accelerates through a summed-and-differential nonsynchronous critical speed just prior to reaching its design point.

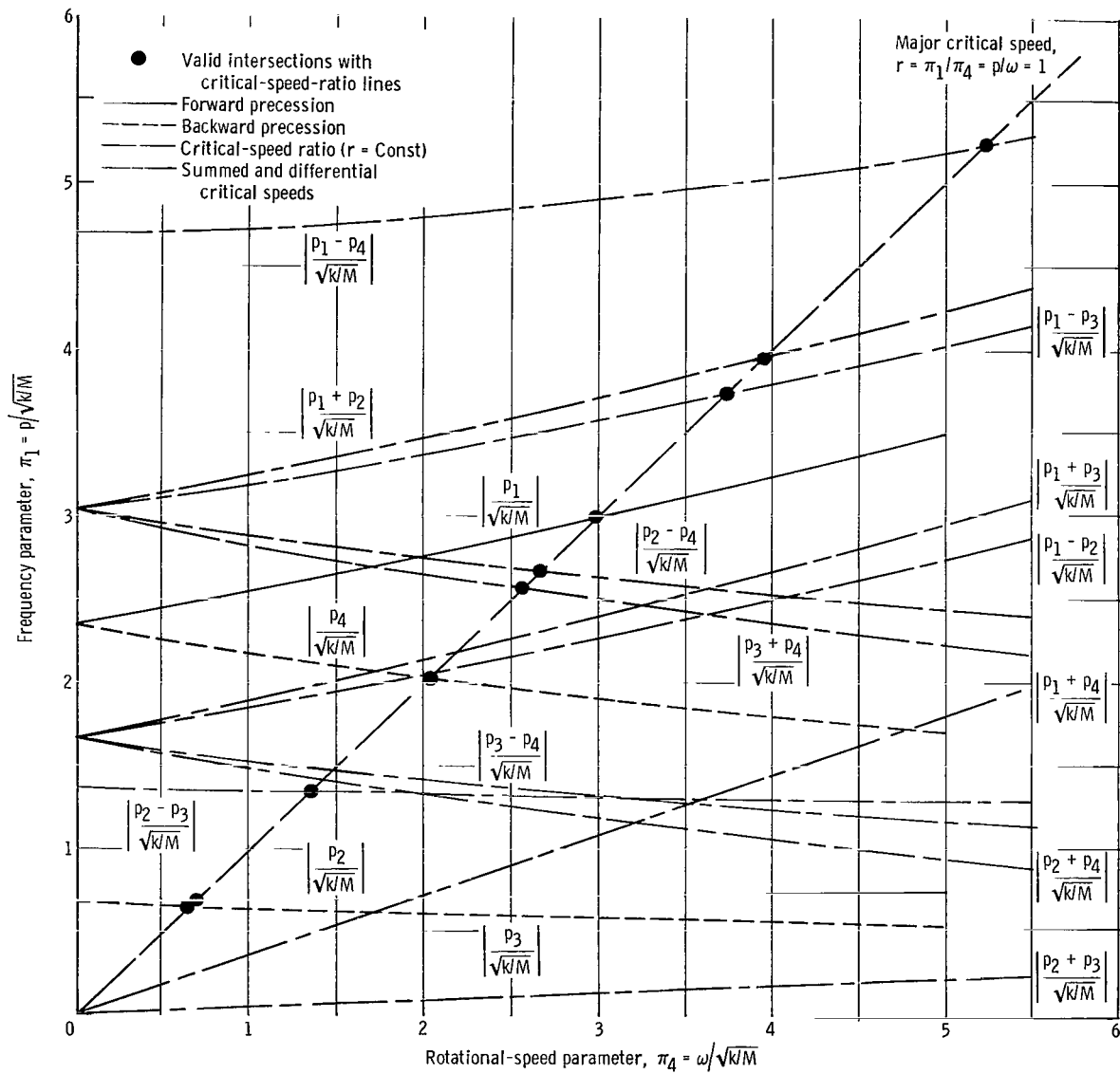Figure 10(a) presents a copy of the $\pi_3 = 0.4$ curve of figure 5(a) with curves of

$$\left| \frac{p_1 \pm p_4}{\sqrt{\dfrac{k\ell^2}{4I_1}}} \right|$$
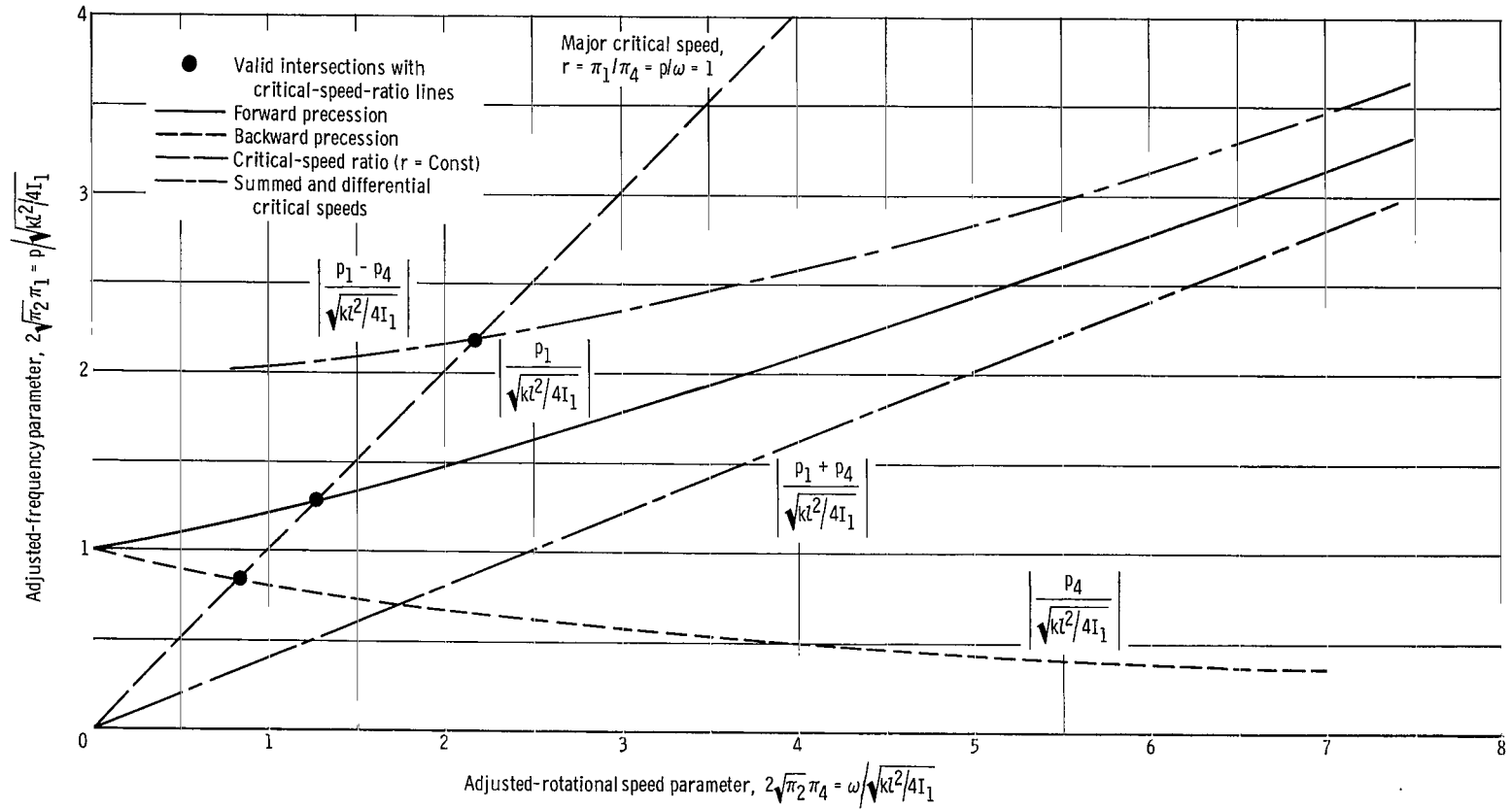
(a) Center of gravity midway between bearings; case 1; $\pi_3 = I/I_1 = 0.4$.

Figure 10. – Summed and differential critical speeds.

(b) Center of gravity at one bearing; case 3; $\pi_2 = I_1/Ml^2 = 0.1$; $\pi_3 = I/I_1 = 0.4$.

Figure 10. – Concluded.

added to illustrate the possibilities for case 1. The uppermost solid circle locates a non-synchronous critical speed at 2.16 for

$$\frac{\omega_{ns}}{\sqrt{\dfrac{k\ell^2}{4I_1}}}$$

This point is established by the intersection of the

$$\left|\frac{p_1 - p_4}{\sqrt{\dfrac{k\ell^2}{4I_1}}}\right|$$

curve with the 45° line through the origin. It is clear that no intersection is possible for the

$$\left|\frac{p_1 + p_4}{\sqrt{\dfrac{k\ell^2}{4I_1}}}\right|$$

curve.

Either equation (B4) or figure 5(a) can be used to show that $\left|p_1 + p_4\right|$ coincides with the line $\left|(p_i \pm p_j)\right|/\omega = 1$ when I/I_1 has a value of 1. From this observation, it is evident that designs having the center of gravity midway between the bearings and $I = I_1$ should be avoided if single-row ball bearings are used because all rotational speeds are critical.

For a rotor with four natural frequencies, as observed for cases 2 to 4, there are twelve summed-and-differential combinations. Figure 10(b) presents a copy from figure 5(c) of the four solutions for case 3 when $\pi_2 = 0.1$ and $\pi_3 = 0.4$. Figure 10(b) also displays all 12 possible $\left|p_i \pm p_j\right|$ combinations.

Because at zero rotor-rotational speed p_1 coincides with p_4 and p_2 coincides with p_3, no $\left|p_1 + p_4\right|$ or $\left|p_2 + p_3\right|$ intersections with the 45° line through the origin of a frequency plot are possible. Figure 10(b), which is drawn for shapes intermediate between pencil shapes and disks, shows 10 $\left|p_i \pm p_j\right|$ intersections with the line $r = 1$. Therefore, the maximum number of intersections for any geometry is 10.

Yamamoto and Hayashi have proved mathematically in reference 10 that only summed

harmonic oscillations can occur if both natural frequencies p_i and p_j represent forward precession or if both represent backward precession. If one frequency represents forward precession and the other, backward, only differential harmonic oscillations can occur. The following tabulations summarize the combinations that can and cannot occur. Can occur:

$$\left.\begin{array}{l} \omega = |p_1 + p_2| \\[1em] \omega = |p_1 - p_3| \\[1em] \omega = |p_1 - p_4| \\[1em] \omega = |p_2 - p_3| \\[1em] \omega = |p_2 - p_4| \\[1em] \omega = |p_3 + p_4| \end{array}\right\} \tag{34}$$

Cannot occur:

$$\left.\begin{array}{l} \omega = |p_1 - p_2| \\[1em] \omega = |p_1 + p_3| \\[1em] \omega = |p_1 + p_4| \\[1em] \omega = |p_2 + p_3| \\[1em] \omega = |p_2 + p_4| \\[1em] \omega = |p_3 - p_4| \end{array}\right\} \tag{35}$$

Valid intersections with the major critical-speed line, according to the allowed combinations of equation (34), are shown by the solid circles in figure 10(b). The four major critical speeds also are located by the appropriate solid circles.

For disks, no intersections for $|p_1 \pm p_j|$ can exist, as figure 5(d) will verify. Therefore, there are five $|p_i \pm p_j|$ intersections with the line $r = 1$ on a frequency plot for a disk. But equation (34) shows that only $|p_2 - p_3|$, $|p_2 - p_4|$, and $|p_3 + p_4|$ can occur

41

for disks. In references 3 and 10, Yamamoto presents experimental evidence to substantiate equations (34) and (35) as applied to disks.

A conclusion from this phase of the study is that the maximum number of summed-and-differential nonsynchronous critical speeds varies from three for a disk to six for pencil shapes.

Plots similar to figure 8 may be drawn for any of the nonsynchronous critical speeds discussed, as well as for the major critical speeds.

SUMMARY OF RESULTS

This rotor critical-speed analysis has yielded the following results when the center of gravity is midway between the bearings:

1. The solution for rotor frequencies simplifies to a single two-branch curve, one for forward and one for backward precession.

2. The forward major critical speed rises rapidly and becomes infinite as the ratio of polar to diametral moments of inertia I/I_1 approaches 1. No forward-precession major critical speeds exist when I/I_1 equals or exceeds 1. The magnitude of backward precession frequency, however, remains finite and decreases slowly throughout the range of I/I_1.

3. Major critical speeds are inversely proportional to $\sqrt{I_1/Ml^2}$ for constant I/I_1.

4. When single-row ball bearings are used, designs should avoid having the polar and diametral moments of inertia equal because a summed-and-differential nonsynchronous critical speed occurs for all rotor rotational speeds.

5. An experimental axial turbopump passes through a major and a nonsynchronous critical speed during acceleration, and at its design point operates close to nonsynchronous critical speeds.

For more general center-of-gravity locations, the following observations were made:

6. A low-frequency set of solutions occurs for forward and backward precession within a band width of -1 to 1 for $p/\sqrt{k/M}$. A high-frequency set occurs outside this band. A no-solution barrier exists at ±1 for $p/\sqrt{k/M}$ except when the center of gravity is centrally located.

7. At any rotor speed of a given configuration, the frequency magnitude of forward precession exceeds that of backward precession.

8. The frequency magnitude of forward precessions increases with increasing rotor speed. The opposite trend occurs for backward precession.

9. As the center-of-gravity location is moved progressively outward, major critical speeds of the low-frequency families decrease in magnitude and those of the high-frequency families increase.

10. In backward precession, disks have lower major critical speeds than pencil shapes.

11. No forward-precession high-frequency critical speeds exist for geometries in which the polar to diametral moment-of-inertia ratio equals or exceeds the critical-speed ratio.

12. The effect of the axial location of the center of gravity on the major critical speeds decreases as geometries become more disk-like.

APPENDIX A

SYMBOLS

A, B, C, D vibration amplitude, m

$\mathscr{D}$ outer diameter of inner ring of ball bearing, m

d diameter of individual ball in ball bearing, m

I rotor polar moment of inertia, $kg\text{-}m^2$

I_1 rotor diametral moment of inertia, $kg\text{-}m^2$

k linear spring constant, kg/sec^2

$\sqrt{k/M}$ natural frequency used for nondimensional purposes, rad/sec

l distance between bearings, m

l_1, l_2 distances from bearings to rotor center of gravity, m

M rotor mass, kg

n general factor in harmonic sequence 1, 1/2, 1/3, ... 1/n

p rotor precession frequency, rad/sec

p_1, p_2, p_3, p_4 rotor precession frequency used in summed-and-differential nonsynchronous critical speeds, rad/sec

r critical-speed ratio, $\pi_1/\pi_4 = p/\omega$

S square of frequency parameter, $(p/\sqrt{k/M})^2$

t time, sec

x axial coordinate of arbitrary reference frame, coincident with shaft centerline when undisturbed, m

y lateral coordinate perpendicular to x-coordinate, m

y_1, y_2 lateral distance from arbitrary reference frame to bearings in y-direction, m

z lateral coordinate mutually perpendicular to x- and y-coordinates, m

z_1, z_2 lateral distance from arbitrary reference frame to bearings in z-direction, m

δ ± 1

π_1 frequency parameter, $p/\sqrt{k/M} = \sqrt{S}$

π_2 dimensionless rotor moment of inertia or disk effect, $I_1/M\ell^2$

π_3 ratio of rotor polar to diametral moment of inertia, I/I_1

π_4 rotor rotational speed parameter, $\omega/\sqrt{k/M}$

ω rotor rotational speed, rad/sec

Subscripts:

B   backward

cr   major critical

F   forward

i, j   dummy indexes, $\left.\begin{array}{l} i = 1, 2, 3, 4 \\ j = 1, 2, 3, 4 \end{array}\right\}$ $i \neq j$

ns   nonsynchronous

45

APPENDIX B

APPLICATIONS

This appendix applies the general solution to the frequency equation (24) to four specific cases. The only variation in these cases is the axial location of the center of gravity.

Center of Gravity Midway Between Bearings (Case 1)

The simplest case is that in which the center of gravity lies midway between the bearings. For this condition (see fig. 1)

$$\frac{l_1}{l} = \frac{l_2}{l} = \frac{1}{2} \tag{B1}$$

Insertion of this relation into equation (24) gives

$$\delta \pi_3 \pi_4 = \sqrt{S} - \frac{1}{4\sqrt{S}\,\pi_2} \tag{B2}$$

It is of great significance that the factor $(S - 1)$ in equation (24) cancels for this case. Basically, it reduces equation (24) from second order in S to first order. By equation (19), equation (B2) is therefore a quadratic in π_1. Rewritten with π_1, equation (B2) is

$$\delta \pi_3 \pi_4 = \pi_1 - \frac{1}{4\pi_1 \pi_2} \tag{B3}$$

If this expression is plotted with π_1 and $\pi_3 \pi_4$ as coordinates, a family of curves with π_2 as the parameter results. More judicious choice of coordinates, however, reduces the family of curves to a single curve. The procedure is to use $\sqrt{\pi_2}$ in each of the two coordinates. Thus

$$\delta 2 \sqrt{\pi_2} \pi_3 \pi_4 = 2\pi_1 \sqrt{\pi_2} - \frac{1}{2\pi_1 \sqrt{\pi_2}} \tag{B4}$$

The coordinates used are

$$2\sqrt{\pi_2}\pi_3\pi_4 = \frac{I}{I_1}\frac{\omega}{\sqrt{\dfrac{k\ell^2}{4I_1}}} \tag{B5}$$

and

$$2\pi_1\sqrt{\pi_2} = \frac{p}{\sqrt{\dfrac{k\ell^2}{4I_1}}} \tag{B6}$$

Den Hartog suggested this technique in reference 8 (p. 259).

The critical speed ratio is defined by

$$r = \frac{\pi_1}{\pi_4} \tag{B7}$$

With this relation, equation (B4) becomes

$$2\sqrt{\pi_2}\,\pi_4 = \frac{1}{\sqrt{r(r - \delta\pi_3)}} \tag{B8}$$

For the major critical speed, defined by equation (27), $r = r_{cr} = 1$, equation (B8) becomes

$$2\sqrt{\pi_2}\,\pi_{4,cr} = \frac{1}{\sqrt{1 - \delta\pi_3}} \tag{B9}$$

Equation (28) also reduces to this form when equation (B1) is used.

In reference 2, Yamamoto observed the following nonsynchronous critical speeds, among others:

Forward precession:

$$r = \frac{1}{2.65} \tag{B10}$$

Backward precession:

$$r = -\frac{1}{4.1} \tag{B11}$$

Use of these expressions and the appropriate value of δ in equation (B4) yields

Forward precession:

$$2\sqrt{\pi_2}\left(\frac{\omega_F}{\sqrt{\frac{k}{M}}}\right) = \sqrt{\frac{2.65}{\frac{1}{2.65} - \pi_3}} \tag{B12}$$

Backward precession:

$$2\sqrt{\pi_2}\left(\frac{\omega_B}{\sqrt{\frac{k}{M}}}\right) = \sqrt{\frac{4.1}{\frac{1}{4.1} + \pi_3}} \tag{B13}$$

Center of Gravity at Quarter Point (Case 2)

If the center of gravity is located one-fourth of the axial distance between the bearings, figure 1 shows that

$$\left.\begin{aligned} \frac{l_1}{l} &= \frac{3}{4} \\[2mm] \frac{l_2}{l} &= \frac{1}{4} \end{aligned}\right\} \tag{B14}$$

With these relations, equation (24) becomes

$$\delta\pi_3\pi_4 = \sqrt{S} - \frac{\frac{5S}{4} - 1}{4\sqrt{S(S-1)}\pi_2} \tag{B15}$$

48

The change-of-coordinate technique used in equation (B4) is of no value in this case because of the S in the numerator of equation (B15); that is, there is no choice of coordinates that can reduce the family of curves to a single curve.

Center of Gravity at One Bearing (Case 3)

When the center of gravity is at one of the bearings, the conditions are

$$\left.\begin{array}{c} \dfrac{l_1}{l} = 1 \\[3mm] \dfrac{l_2}{l} = 0 \end{array}\right\} \tag{B16}$$

then

$$\delta\pi_3\pi_4 = \sqrt{S} - \frac{2S - 1}{4\sqrt{S(S-1)}\pi_2} \tag{B17}$$

This expression also results in a family of curves with π_2 as parameter.

Center of Gravity at Outboard Quarter Point (Case 4)

The relations among l_1, l_2, and l for this case are

$$\left.\begin{array}{c} \dfrac{l_1}{l} = \dfrac{5}{4} \\[3mm] \dfrac{l_2}{l} = -\dfrac{1}{4} \end{array}\right\} \tag{B18}$$

The solution to the frequency equation is

$$\delta\pi_3\pi_4 = \sqrt{S} - \frac{\dfrac{13S}{4} - 1}{4\sqrt{S(S-1)}\pi_2} \tag{B19}$$

49

REFERENCES

1. Gunter, Edgar J., Jr.: Dynamic Stability of Rotor-Bearing Systems. NASA SP-113, 1966.

2. Yamamoto, Toshio: On the Critical Speeds of a Shaft. Memoirs Faculty Eng., Nagoya University, vol. 6, no. 2, Nov. 1954, pp. 106-174.

3. Yamamoto, Toshio: On the Vibrations of a Rotating Shaft. Memoirs Faculty Eng., Nagoya University, vol. 9, no. 1, May 1957, pp. 19-115.

4. Dimentberg, F. M.: Flexural Vibrations of Rotating Shafts. Butterworths Scientific Publications, 1961.

5. Eshleman, R. L.; and Eubanks, R. A.: On the Critical Speeds of a Continuous Shaft-Disk System. Paper No. 67-Vibr-9, ASME, Mar. 1967.

6. Graham, Robert D.; Rowan, B. F.; and Shen, F. A.: Axial Pump Rotordynamic Study. Rep. No. R-6982 (NASA CR-72302), Rocketdyne Div., North American Aviation, Oct. 1, 1967.

7. Timoshenko, S.; and Young, D. H.: Vibration Problems in Engineering. Third ed., D. Van Nostrand Co., Inc., 1966.

8. Den Hartog, J. P.: Mechanical Vibrations. Fourth ed., McGraw-Hill Book Co., Inc., 1956.

9. Yamamoto, Toshio: On Critical Speeds of a Shaft Supported by a Ball Bearing. J. Appl. Mech., vol. 26, no. 2, June 1959, pp. 199-204.

10. Yamamoto, Toshio; and Hayashi, Satoru: Summed and Differential Harmonic Oscillations in Nonlinear Vibratory Systems. Memoirs Faculty Eng., Nagoya University, vol. 18, no. 2, Nov. 1966, pp. 85-150.

FIRST CLASS MAIL

"The aeronautical and space activities of the United States shall be conducted so as to contribute . . . to the expansion of human knowledge of phenomena in the atmosphere and space. The Administration shall provide for the widest practicable and appropriate dissemination of information concerning its activities and the results thereof."

— NATIONAL AERONAUTICS AND SPACE ACT OF 1958

NASA SCIENTIFIC AND TECHNICAL PUBLICATIONS

TECHNICAL REPORTS: Scientific and technical information considered important, complete, and a lasting contribution to existing knowledge.

TECHNICAL NOTES: Information less broad in scope but nevertheless of importance as a contribution to existing knowledge.

TECHNICAL MEMORANDUMS: Information receiving limited distribution because of preliminary data, security classification, or other reasons.

CONTRACTOR REPORTS: Scientific and technical information generated under a NASA contract or grant and considered an important contribution to existing knowledge.

TECHNICAL TRANSLATIONS: Information published in a foreign language considered to merit NASA distribution in English.

SPECIAL PUBLICATIONS: Information derived from or of value to NASA activities. Publications include conference proceedings, monographs, data compilations, handbooks, sourcebooks, and special bibliographies.

TECHNOLOGY UTILIZATION PUBLICATIONS: Information on technology used by NASA that may be of particular interest in commercial and other non-aerospace applications. Publications include Tech Briefs, Technology Utilization Reports and Notes, and Technology Surveys.

Details on the availability of these publications may be obtained from:

SCIENTIFIC AND TECHNICAL INFORMATION DIVISION

NATIONAL AERONAUTICS AND SPACE ADMINISTRATION

Washington, D.C. 20546